



1 Does a convection-permitting regional climate
2 model bring new perspectives on the projection of
3 Mediterranean floods?
4

5 Nils Poncet¹

6 Philippe Lucas-Picher^{1,2}

7 Yves Trambly³

8 Guillaume Thirel^{1,4}

9 Humberto Vergara^{5,6}

10 Jonathan Gourley⁵

11 Antoinette Alias¹

12

13 1 Centre National de Recherches Météorologiques (CNRM), Université de Toulouse, Météo-
14 France, CNRS, Toulouse, France

15

16 2 Département Des Sciences de La Terre Et de L'atmosphère, Université du Québec À
17 Montréal, Montréal, QC, Canada

18

19 3 HSM, Univ. Montpellier, CNRS, IRD, Montpellier, France

20

21 4 Université Paris-Saclay, INRAE, HYCAR Research Unit, Antony, France

22

23 5 Cooperative Institute for Severe and High-Impact Weather Research and Operations,
24 University of Oklahoma, Norman, Oklahoma, USA

25

26 6 NOAA/National Severe Storms Laboratory, Norman, Oklahoma, USA

27

28

29 Correspondence to: Nils Poncet (nilsponcet@hotmail.fr)

30

31

32

33

34



35 **Abstract**

36

37 Floods are the primary natural hazard in the French Mediterranean area causing damages
38 and fatalities every year. These floods are triggered by heavy precipitation events (HPEs)
39 characterized by limited temporal and spatial extents. A new generation of regional climate
40 models at the kilometer scale have been developed, allowing an explicit representation of
41 deep convection and improved simulations of local-scale phenomena such as HPEs.
42 Convection-Permitting regional climate Models (CPMs) have been scarcely used in
43 hydrological impact studies, and future projections of Mediterranean floods remain uncertain
44 with Regional Climate Models (RCMs). In this paper, we use the CNRM-AROME CPM (2.5
45 km) and its driving CNRM-ALADIN RCM (12 km) at the hourly timescale to simulate floods
46 over the Gardon at Anduze catchment located in the French Mediterranean region. Climate
47 simulations are bias-corrected with the CDF-t method. Two hydrological models, a lumped
48 and conceptual model (GR5H), and a process-based distributed model (CREST), forced with
49 historical and future climate simulations from the CPM and from the RCM, have been used.
50 The CPM model confirms its ability to better reproduce extreme hourly rainfall compared to
51 the RCM. This added value is propagated on flood simulation with a better reproduction of
52 flood peaks. Future projections are consistent between the hydrological models, but differ
53 between the two climate models. With the CNRM-ALADIN RCM, all floods are projected to
54 increase, whereas a threshold effect is found for simulations driven by the CNRM-AROME
55 CPM, where the magnitude of the largest floods is expected to increase while the moderate
56 floods are expected to decrease. In addition, different flood event characteristics indicate that
57 floods are expected to become flashier in a warmer climate, regardless of the model. This
58 study is a first step for impact studies driven by CPMs over the Mediterranean.

59

60

61

62

63

64

65

66

67

68

69

70

71



72 1. Introduction

73

74 Every year, the French Mediterranean region faces intense flash floods during the fall season
75 causing important damages and casualties. Even if only small to medium catchments are
76 concerned, flash floods are amongst the most destructive hazards in the French
77 Mediterranean region (Boudou et al., 2016; Vinet et al., 2022). These hydrological events are
78 triggered by Heavy Precipitation Events (HPEs) that can bring up to half of the annual rainfall
79 in a few hours to days (Delrieu et al., 2005; Nuissier et al., 2011; Ricard et al., 2012). Initiated
80 by the complex interaction between moisture fluxes from the Mediterranean Sea to the
81 atmosphere, synoptic scale processes and topography, HPEs are complex and challenging to
82 simulate and forecast with precision (Khodayar et al., 2018; Caillaud et al., 2021; Caumont et
83 al., 2021). Due to their strong societal and economic impacts, being able to model HPEs and
84 their resulting flash floods in current and future climate is an important societal concern.

85

86 For several decades, faster computational capabilities and improved understanding of
87 atmospheric processes have enhanced the confidence towards climate model simulations at
88 global and regional scales (Rummukainen, 2010; Giorgi, 2019). Using a limited area, Regional
89 Climate Models (RCMs) can reach spatial resolutions down to 10 km by dynamically
90 downscaling global climate model (GCM) simulations (Giorgi and Gutowski, 2015). The
91 increase of climate model spatial resolutions with time brought a more accurate description of
92 the topography and an improved simulation of physical processes, improving the simulation
93 of regional meteorological phenomena such as extreme rainfall events (Giorgi, 2019). Due to
94 their higher spatial resolutions, RCMs allow the study of climate change impacts at the regional
95 scale (Maurer et al., 2007; Teutschbein and Seibert, 2010). Namely, numerous studies have
96 used RCM simulations as inputs for hydrological models to simulate discharge and floods in
97 Europe (Kay et al., 2006; Dankers and Feyen, 2009; Köplin et al., 2014). Often necessary for
98 hydrological simulations, bias correction methods can substantially affect the projection of
99 floods in a warmer climate (Boé et al., 2007; Rojas et al., 2011; Teutschbein and Seibert,
100 2012).

101

102 RCM projections generally agree on the increase of extreme precipitation in the French
103 Mediterranean region (Tramblay and Somot, 2018; Zittis et al., 2021), confirming the observed
104 trends (Ribes et al., 2019). Despite the positive trends in rainfall extremes over the French
105 Mediterranean region, the link of this signal on floods is not straightforward (Sharma et al.,
106 2018; Tramblay et al., 2019). Hydrological trends depend on multiple factors, such as
107 catchment location, event severity, flood generating processes and soil moisture conditions
108 (Blöschl et al., 2019; Wasko et al., 2023; Brunner et al., 2021). In the Mediterranean area, the
109 reduction of the soil moisture prior to flood events could counterbalance rainfall extremes and
110 possibly invert the sign of observed flood changes (Tramblay et al., 2023). In terms of future
111 trends, the signal on floods magnitude and frequency thus remains uncertain in the French
112 Mediterranean region. Using daily variables from an RCM ensemble, Alfieri et al. (2015)
113 showed a future decrease in mean annual flows and an increase of flood frequency in this
114 area. Thober et al. (2018) showed a decrease of high flows and flood magnitudes for different
115 levels of future global warming. On the contrary, Lemaitre-Basset et al. (2021) reported a
116 projected increase in flood severity in southern France.

117



118 Under a Mediterranean climate, precipitation is usually the main driver for runoff production.
119 Floods are therefore mainly triggered by HPEs on small catchments (Amponsah et al., 2018).
120 Despite RCMs' good simulation of climatic conditions, biases remain in the representation of
121 some regional and local phenomena, such as HPEs (Khodayar et al., 2016; Caillaud et al.,
122 2021). Indeed, with resolutions coarser than 10 km, the simulation of convective events with
123 RCMs requires the use of deep convection parameterization schemes, leading to an
124 underestimation of rainfall extremes (Prein et al., 2016; Ban et al., 2021). This poor
125 representation of sub-daily extreme rainfall by RCMs could question the reliability of the flood
126 impact studies over small Mediterranean catchments, perhaps explaining some contradictory
127 results identified in the literature.

128
129 During the last decade, a new generation of RCMs has emerged (Kendon 2010). Convection-
130 permitting regional climate models (CPMs) have a resolution finer than 4 km. Their resolution
131 is sufficiently fine to allow an explicit representation of deep convective processes (Lucas-
132 Picher et al., 2021) and thus to get rid of deep convection parameterization schemes, which
133 are necessary in RCMs. Most of the studies using CPMs show a clear added value compared
134 to RCMs in the representation of local-scale phenomena such as convective cells and
135 localized intense precipitation (Prein et al., 2015; Coppola et al., 2020; Caillaud et al., 2021;
136 Ban et al., 2021; Caldas-Alvarez et al., 2022). In the context of the COordinated Regional
137 climate Downscaling EXperiment Flagship Pilot Study (CORDEX-FPS) convection initiative,
138 Ban et al. (2021) carried out a multimodel evaluation of CPMs over a central European domain.
139 This study confirmed the added value of different CPMs in the simulation of hourly extreme
140 precipitation.

141
142 Even if CPMs are a promising tool to study hydrological impacts, only a few of them have yet
143 been used for this purpose. Results from these preliminary studies do not indicate
144 improvements in discharge simulation and flood modeling using CPMs. Kay et al. (2015) used
145 a CPM output to feed a hydrological model over river basins in Great Britain. Their results
146 indicate no added value using this CPM on discharge modeling, with strong geographical
147 differences. The same conclusion was found by Reszler et al. (2018) using CCLM and WRF
148 CPM simulations as input for the KAMPUS distributed hydrological model over a continental
149 and mountainous domain (Eastern Alps). Mendoza et al. (2016) compared the impact of
150 climate model spatial resolution in Colorado, showing the ability of CPMs to reproduce
151 observed annual cycles especially in mountainous catchments. In an idealized modeling chain
152 with different climate simulation resolution, Quintero et al. (2021), found that a 4-km grid
153 spacing CPM is the best compromise between computational costs and performance of
154 hydrological modeling. In terms of future projections, and using CPMs as an input of a
155 distributed hydrological model, floods are projected to become more severe, more frequent,
156 more unpredictable and flashier in the USA (Li et al., 2022a, b). In a recent study, Kay (2022)
157 used an ensemble of CPMs to feed a gridded hydrological model, showing a better
158 performance and higher future flow changes of CPMs compared to RCMs. Using a modeling
159 chain driven by a CPM over a tropical area in Africa, Ascott et al. (2023) indicate no significant
160 trend in floods in future projections. Even though the aforementioned studies have pioneered
161 the use of CPMs with hydrological models, they are limited to only one hydrological model,
162 ignoring uncertainty induced by hydrological model discrepancies. To our knowledge, no
163 paper has studied Mediterranean floods using a CPM.

164



165 In this study, we would like to assess the added value of a CPM regarding the evolution of
166 floods over a Mediterranean catchment prone to intense floods. For this, we perform an
167 analysis of simulated floods magnitudes and characteristics under a historical scenario and
168 under the RCP 8.5 emission scenario. Two climate datasets, a CPM (CNRM-AROME) and its
169 driving RCM (CNRM-ALADIN), are used as inputs to one lumped, conceptual hydrological
170 model (GR5H) and one distributed, process-based hydrological model (CREST used in EF5).

171 The main aims of this paper are to:

- 172 • Evaluate the added value of the CPM on extreme rainfall at the scale of a small
173 Mediterranean basin
- 174 • Evaluate the capacity of a CPM to reproduce Mediterranean floods using two
175 hydrological models
- 176 • Assess future changes in floods distributions and characteristics between the two
177 models and two climate simulations

178 Section 2 describes the area of interest, the data and the different climate and hydrologic
179 models. The methodology is detailed in Sect. 3. The evaluation of the climate and hydrological
180 models and the projection of floods are presented and discussed in Sect. 4.

181

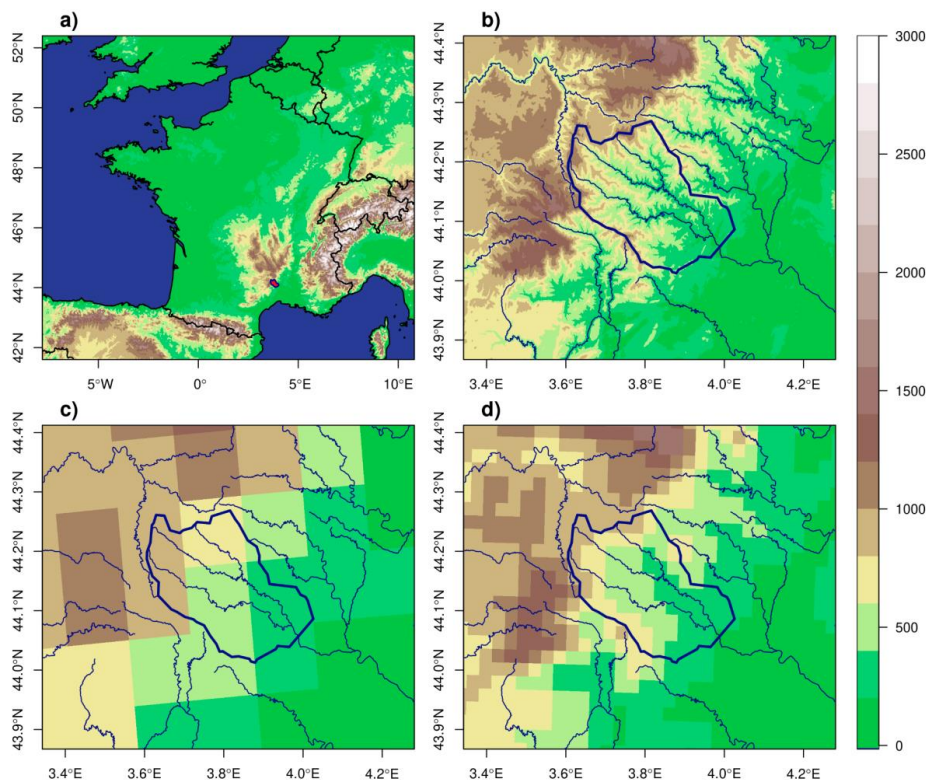
182 2. Study area and data

183

184 2.1. Catchment: Gardon d'Anduze

185

186 The study is performed over a 543 km² Mediterranean catchment, the Gardon d'Anduze,
187 located in the Cévennes region, on the southern slopes of the Massif Central Mountain range.
188 The Gardon d'Anduze has a complex topography ranging from 130 m to 1200 m a.s.l.
189 Consequently, it is a rather natural, forested and lightly urbanized. Indeed, most of its surface
190 is covered by typical Mediterranean vegetation. The soils are relatively thin, from 10 cm at the
191 top of the hillslopes to 100 cm close to the river bed (Vannier et al., 2014). It is considered as
192 a highly reactive Mediterranean catchment, known for experiencing some of the most
193 destructive flash floods in France (Delrieu et al., 2005; Toukourou et al., 2011). The Gardon
194 d'Anduze catchment has been extensively studied due to its location of particular interest in
195 hydrology, especially for flash flood modeling and forecasting (Alfieri et al., 2011; Roux et al.,
196 2011; Moussa, 2010). Figure 1 displays the location of Gardon d'Anduze in France (a), and
197 orography as shown by a 80-m resolution DEM (b), and by the RCM and CPM (c and d).



198

199 **Figure 1: Location of Gardon d'Anduze catchment (in red) over France (a), orography**
200 **of this catchment represented by a 80-m DEM (b), by the 12-km CNRM-ALADIN RCM(c)**
201 **and the 2.5-km CNRM-AROME CPM (d)**

202

203 2.2. Climate models

204 In this study, we use climate simulations from a CPM and its forcing RCM, both developed
205 and released at the Centre National de Recherches Météorologiques (CNRM), in Toulouse,
206 France. Information about these two climate models is summarized in Table 1.

207

208 CNRM-ALADIN is a 12-km grid cell RCM that has been run over the continental EUR-11
209 domain through the EURO-CORDEX initiative. Retrospective simulations are driven by the
210 ERA-Interim global reanalysis dataset (Dee et al., 2011), while historical and future scenarios
211 are forced by the CNRM-CM5 global model (Voldoire et al., 2013). This version is derived from
212 the development of the NWP model ALADIN, thanks to the ACCORD research centers
213 consortium. CNRM-ALADIN has been extensively used in the CORDEX framework over
214 Europe, Mediterranean, North America and Africa. For more details about the parametrization
215 schemes and configurations of the last version of ALADIN, see Nabat et al., 2020 and Lucas-
216 Picher et al., 2023.



217 CNRM-AROME is a CPM, which is adapted from the cycle 41 of the NWP AROME formerly
218 operating for numerical weather prediction. Simulations used in this study are produced over
219 the NW domain, covering France, the UK, North of Spain and most of Germany with a 2.5-km
220 mesh. Some papers have already evaluated this model, under a former release (Fumière et
221 al., 2020), a different domain and forcing RCM version (Caillaud et al., 2021), or the same
222 version and domain used in this study (Lucas-Picher et al., 2023). All these evaluations have
223 established the added value of CNRM-AROME in the reproduction of extreme rainfall and
224 HPEs compared to CNRM-ALADIN over the domains. To our knowledge, no published study
225 has used CNRM-AROME projections for climate change assessment.
226 In this paper, ALADIN and AROME refer to the version of CNRM-ALADIN and CNRM-AROME
227 described above, respectively.
228
229

	CNRM-ALADIN	CNRM-AROME
Version	6.3	41t1
Resolution	12 km	2.5 km
Retrospective simulation (evaluation)	1979-2018	2000-2018
Historical simulation	1951-2005	1986-2005
Future simulation (RCP 8.5)	2006-2100	2080-2099
Deep convection	parameterized	explicit
Reference papers	Nabat et al., 2020	Lucas-Picher et al., 2023

230 **Table 1 : Information about the two climate models and their associated simulations**
231 **used in this study**
232

233 2.3. Observations

234
235 In this study, we compare the hourly simulated data with a high-resolution observed
236 precipitation dataset so-called COMEPHORE. COMEPHORE is an hourly 1-km resolution
237 gridded product covering the Metropolitan French during the 1997-2019 period.
238 COMEPHORE was built by merging weather station rainfall measurements and different radar
239 sources (Laurantin et al., 2012; Caillaud et al., 2021). The dataset used approximately 3000
240 daily rain gauges and 1200 hourly rain gauges. The number of radars have more than doubled
241 during the first decade of data. In 2019, COMEPHORE was built using data from 29 radars
242 comprising the French radar network (ARAMIS), in addition to foreign radars such as those
243 from the Swiss network and one on Jersey Island. Even though the quality of the dataset is
244 not temporally and spatially homogeneous, COMEPHORE is still considered as the best
245 national reference for studying hourly rainfall at high spatial and temporal resolutions.
246 Furthermore, the Gardon d'Anduze river catchment is located in a region of high rain gauges
247 and radar density, raising the confidence in this dataset for a benchmark in this study (Caillaud
248 et al., 2021). Temperature is the main variable to compute potential evapotranspiration (PET).



249 As a reference, we extracted 3-h temperature measurements from 6 weather stations in the
250 basin. Temperature was then linearly downscaled to the hourly time step and interpolated over
251 the catchment using an inverse distance weighting method.

252
253 Numerous methods exist to compute PET from climatic variables for hydrological modeling
254 perspectives (Oudin et al., 2005). Here, we compute PET using the Hargreaves-Samani (HS)
255 method (Hargreaves and Samani, 1982). We chose a reliable, widespread applied method
256 that requires the minimum amount of climate variables at the daily time step. Daily PET is then
257 disaggregated to the hourly time step using a standard distribution curve as done in Lobligeois,
258 2014. We applied the same methodology for simulated temperature.
259

260 2.4. Hydrological models

261
262 Two hydrological models with different physical concepts were used in this framework. This
263 choice was made to consider the potential uncertainty related to hydrological modeling that
264 can affect hydrological projections (see e.g. Lemaitre-Basset et al., 2021, that discusses this
265 issue for the neighboring Hérault catchment).

266
267 The GR5H model is a lumped, conceptual rainfall-runoff model that runs hourly (Ficchi et al.,
268 2019). Based on several conceptual reservoirs, such as a soil-moisture accounting reservoir,
269 and a unit hydrograph, this model transforms catchment-aggregated hourly precipitation and
270 potential evapotranspiration data into simulated hourly discharge. The GR5H model takes into
271 account the interception of rainfall by vegetation, which was proven important for flood events
272 (Ficchi et al., 2019). The GR5H model parameters were calibrated against observed discharge
273 using the NSE objective function. This model or close versions belonging to the so-called GR
274 family of hydrological models have been used both for flood simulation (Ficchi et al., 2019;
275 Astagneau et al., 2021), and climate change applications (Chauveau et al., 2013; Lemaitre-
276 Basset et al., 2021). The GR5H model was run using the open source airGR R package (Coron
277 et al., 2017, 2020), which also provides the parameter calibration algorithm that was used.

278
279 The Ensemble Framework For Flash Flood Forecasting (EF5) is a software for distributed
280 water balance modeling (Flamig et al., 2020), including different schemes for runoff production
281 and routing. As part of EF5, we used the Coupled Routing and Excess Storage (CREST)
282 model and the kinematic wave routing scheme, at the hourly time step. CREST is a fully
283 distributed model, process-based hydrological model. It can be defined as a hybrid between
284 a conceptual and a physics-based model (Wang et al., 2011). All hydrological processes, such
285 as runoff production, evapotranspiration and sub-grid cell routing are computed at each grid
286 cell. CREST is composed of two excess storage reservoirs, one for interception by the
287 vegetation canopy and one representing a layer of soil. For each cell, runoff and infiltration are
288 separated using a variable infiltration curve. Therefore, this model takes into account the two
289 main runoff production mechanisms: saturation-excess and infiltration-excess. The
290 subsurface routing is done with a linear reservoir model. Total runoff, composed of surface
291 and sub-surface runoff water, is then routed to the outlet following the orography provided by
292 a digital elevation model (DEM) with the kinematic wave routing scheme. Actual
293 evapotranspiration is determined in the model from PET input and the water content of the
294 cell. The CREST model is composed of 13 parameters: 6 for runoff production and 7 for the



295 routing. Here we will refer to this adaptation of CREST in EF5 simply as CREST for
296 succinctness. The DiffeRential Evolution Adaptive Metropolis (DREAM) scheme is used for
297 automatic calibration to estimate the best parameter set (Vrugt et al., 2009). A complete
298 description of parameters is provided in Flamig et al., 2020. CREST is a model initially
299 developed to respond to the need of forecasting floods at the global scale (Wang et al., 2011),
300 but is perfectly suitable to simulate flash floods (Flamig et al., 2020) through EF5. Indeed,
301 CREST has been used to study extreme hydrological events; for example to reproduce floods
302 from a major hurricane event (Li et al., 2021) or floods and flash floods in a warmer future (Li
303 et al., 2022b, a). In this study, topographic data from the version 1.1 of HydroSHED database
304 is used for CREST. Resolution of the DEM is 15 arc-sec, hence for this latitude around 300 m
305 in longitude by 450 m in latitude. Drainage direction maps and flow accumulation maps are
306 then produced using the QGIS software and packages.

307

308 The CREST and GR5H hydrological models have been calibrated using the hourly observed
309 discharge from 2002-2018, using the COMEPHORE hourly rainfall dataset and PET computed
310 from observed air temperatures. For GR5H, all the model parameters have been calibrated.
311 For CREST, most parameters have been fixed (Li et al., 2022b) and the calibration has been
312 performed on a few sensitive parameters. The Nash and Sutcliffe Efficiency (NSE) criteria is
313 used as an objective function for the calibration process. We initialized the models during a
314 one-year warmup period before the starting date. Both hydrological models have been
315 evaluated using the following metrics (see Sect. 4.2) over the 2002-2018 period:

316

- 317 • Nash and Sutcliffe Efficiency (Nash and Sutcliffe, 1970)
- 318 • KGE (Gupta et al., 2009)
- 319 • Bias on mean flows
- 320 • Bias on quantile 99.9
- 321 • Bias on Peak Over Thresholds (POT) distributions: we compared the mean of
322 simulated POT distribution to the mean of observed POT distribution.

323

324 The same period (2002-2018) is kept to run the hydrological models driven with retrospective
325 climate simulations. For the scenarios datasets, using a 1-year warmup period, we computed
326 simulations over two epochs of 19 years for historical (1987-2005) and future (2081-2099)
327 periods.

328

329

330

331

332

333

334

335

336

337

338

339



340 3. Methods

341

342 3.1. Bias correction

343

344 Climate simulations, and notably precipitation, often show significant biases that prevent their
345 direct use in impact studies using hydrological models. Indeed, hydrological models are
346 calibrated over climatic conditions that can differ strongly from the raw historical climate
347 simulations. The use of bias correction methods on climate simulations is an open debate
348 (Addor and Seibert, 2014; Huang et al., 2014; Maraun, 2016). However, correction of biased
349 climate simulations is widely used for hydrological impact studies and future projections
350 (Reszler et al., 2018; Giorgi, 2019; Lucas-Picher et al., 2021).

351

352 In order to correct simulated climate data biases, we used an univariate statistical bias
353 correction method. CDF-t is a statistical bias correction method specifically developed for
354 correcting biases of climate variables (Michelangeli et al., 2009). The basis of this method is
355 an extension of a quantile mapping method that allows a change of distribution statistics for
356 corrected variables. Consequently, CDF-t is particularly appropriate to correct future climate
357 datasets in a non-stationary climate (Michelangeli et al., 2009; Vrac et al., 2012) and it is
358 largely used to correct future climate projections for the sake of climate change impact studies.
359 In this study, we applied the CDF-t correction on hourly precipitation and temperature
360 variables. Due to the distinct seasonality of precipitation, and a strong spatial variability of
361 precipitation in this catchment, we corrected simulated datasets for each calendar month and
362 over each grid cell separately. To take into account differences in the ratio of wet and dry
363 hours, the Singularity Stochastic Removal (SSR) preprocessing method is applied for
364 precipitation simulations (Vrac et al., 2016). Historical simulations are corrected against the
365 corresponding observed period (2000-2018). With the common period of data between
366 observations and historical AROME simulations being relatively short (8 years), we chose to
367 correct observations and the historical simulation over two asynchronous periods of same
368 length, respectively 2000-2019 and 1986-2005. This correction is then applied over the end of
369 century RCP 8.5 projections (2080-2099). All these operations are performed through the R
370 package SBCK (Robin, 2022). For the GR5H model, corrected climate outputs are then
371 averaged over the Gardon d'Anduze catchment.

372 3.2. POT extraction and declustering

373

374 This study focuses on floods. To extract floods from discharge time series, two approaches
375 are widely adopted: the maximum annual discharge flood (AMF) and a Peak Over Threshold
376 (POT) extraction (Lang et al., 1999). The POT selection method consists of the extraction of
377 all flood peaks exceeding a threshold. Contrary to the AMF method, the POT method
378 preserves the hydrological information especially in Mediterranean catchments where several
379 flash floods can occur every year. Hence, we selected this method for flood extraction in this
380 paper. The POT method requires temporal independence between flood peaks. To ensure
381 this assumption, a declustering algorithm has been developed and applied to evaluate
382 temporal dependencies between POTs, adapted from Lang et al. (1999). The declustering
383 applied herein considers that two floods are independent if there is a minimum duration of 96



384 hours between the two events, and if the discharge between different events must drop below
385 75 % of the minimum value of the flood peaks.

386

387 Cunnane (1973) found that the POT method minimizes the sampling variance for a threshold
388 producing on average 1.65 flood peaks per year, compared to the AMF. To get a sufficient
389 sample of simulated POT (in particular for ALADIN), we fixed here the discharge threshold to
390 have an average of two floods per year for the observed discharge (corresponding to a
391 threshold equal to $265 \text{ m}^3 \cdot \text{s}^{-1}$), after declustering.

392

393 3.3. Flood characteristics

394 For each event, several flood characteristics and their associated rainfall events are also
395 analyzed. These metrics aim to understand future changes in flood mechanisms as projected
396 by climate simulations. For instance, changes in flood peak baseflow can give information on
397 change in antecedent soil moisture. The Lag-time and flashiness indexes describe the
398 intensity and speed of the rise of the river flow, a signature of potential catastrophic impacts
399 (flash flood). At the same time, characteristics of the rainfall events (duration, intensity,
400 maximum) in tandem with the flood characteristics help elucidate the driving processes and
401 causes of future changes in the basin's hydrometeorology. Rainfall events associated with
402 each POT (Sect. 3.2) are defined by a sequence of hourly rainfall prior to the flood peak (i)
403 interrupted by no more than 2 dry hours and (ii) yielding at least 30 mm to trigger the
404 hydrological event. These two conditions have been tested for different values with observed
405 datasets, and have shown very little sensitivity to defining the flood characteristics. The rainfall
406 thresholds are related to our knowledge of the river basin dynamics and hydrological expertise.
407 Table 1 summarizes metrics names, meaning and computation details.

408

409

410

411

412

413

414

415

416

417

418

419

420

421

422

423

424

425

426

427

428

429



430
 431
 432

Metric name	Definition	Equation
n_p	Duration of rainfall event (h)	
P_{max}	Maximum hourly precipitation of rainfall events associated with the flood (mm)	$P_{max} = \max(P_i)$ i are temporal indices of rainfall event
P_{tot}	Rainfall event total amount (mm)	$P_{tot} = \sum_1^{n_p} P_i$
B_{POT}	Baseflow value ($\text{m}^3 \cdot \text{s}^{-1}$) at the flood peak timestep. Baseflow timeseries are extracted from the R package hydroEvents with default filter values (Wasko and Guo, 2022)	
R_{POT}	Baseflow contribution of the POT (%)	$R_{POT} = \frac{B_{POT}}{Q_{POT}}$
n_Q	Duration of flood event (h)	$n_Q = n + 1$ with n number of timesteps exceeding the threshold
L_T	Lag time (h), reactivity (concentration time) of the catchment for the given hydro-meteorological event. Time difference between the rainfall event centroid and the POT. To remove artifacts, and for consistency issues, a temporal window of 24 h prior to the POT was chosen.	$j_{centroid} = \frac{\sum_{q-24}^q j P_j}{\sum_{q-24}^q P_j}$ with j : indices of flood event $q = j_{POT}$ the index of POT $L_T = q - j_{centroid}$
F_I	Flashiness Index (-): Flashiness of flood determined by a combination of flood reactivity and magnitude, proxy of flood severity. Adapted from Li et al., 2022.	$F_I = \frac{Q_{POT} - B_{POT}}{L_T}$

433 **Table 1 : Flood characteristics definition and details**

434
 435



436 4. Results and discussion

437 4.1. Added value of CPM at the catchment scale

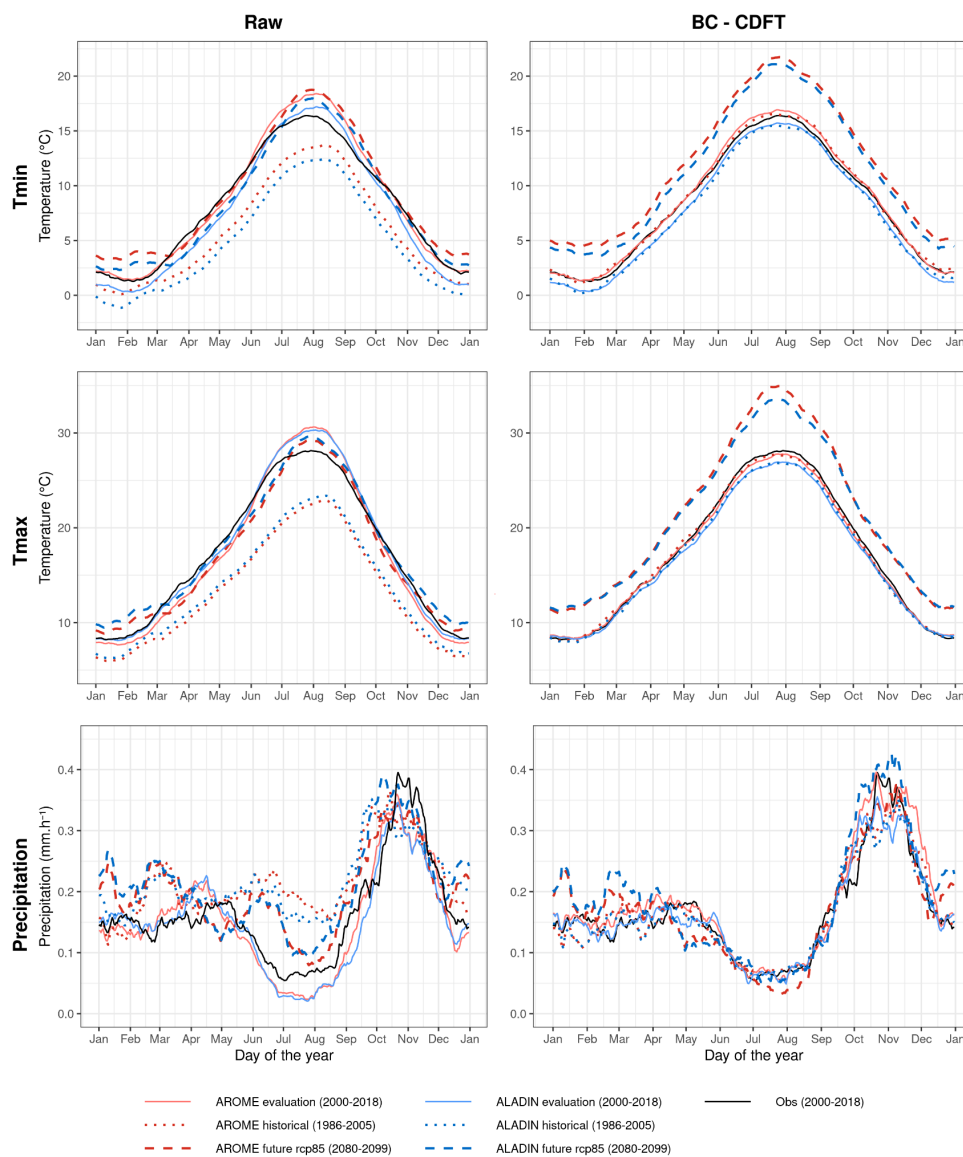
438

439 We first analyze the climate datasets aggregated at the scale of Gardon d'Anduze catchment.
440 Figure 2 shows the annual cycle for daily minimum (Tmin) and maximum (Tmax) temperature
441 and hourly precipitation, before (raw) and after bias correction (BC-CDFT).
442 AROME and ALADIN in retrospective mode (evaluation) show correct annual cycles despite
443 an overestimation of summer temperature both for Tmin and Tmax. Results in this area are in
444 line with the recent evaluation of the ALADIN and AROME climate models (Lucas-Picher et
445 al., 2023). The ALADIN RCM is generally colder than AROME, which can be explained by an
446 effect of resolution. A strong cold bias (3-5 °C) is visible over all seasons for both models in
447 historical scenarios over the period 1986-2005. This cannot be explained by climate variability
448 or by climate change signals between the decades 1986-2005 and 2000-2018. This is a known
449 cold bias of climate models driven by the GCM CNRM-CM5 (Vautard et al., 2021). Annual
450 cycles for Tmin and Tmax for future projections (RCP 8.5) are similar to the evaluation period,
451 i.e climate change signals for temperature are almost of the same magnitude as the cold bias.
452 As expected, this cold bias disappears after bias correction for both AROME and ALADIN
453 historical scenarios. The bias-corrected temperatures under the RCP 8.5 scenario strongly
454 increase for all seasons. However, the strongest signal is seen for the summer months.

455

456 Annual cycles of precipitation are well reproduced for ALADIN and AROME for the evaluation
457 period. Both models are a bit too wet in spring and too dry in summer, but the wet season
458 (October to December) on simulations is clearly distinguishable and identical to COMEPHORE
459 dataset (observations). The wet bias in spring can deeply affect soil moisture state in the
460 hydrological models and therefore probably lead to a change in the behavior of the first floods
461 occurring during the autumn months. The two climate models are able to reproduce the
462 precipitation seasonality. There is no evidence of added value from the CPM on the simulation
463 of the annual cycle of precipitation on this catchment. Results are similar for AROME and
464 ALADIN for historical projections: spring and summer seasons are too wet. This causes a
465 weaker annual cycle of precipitation. The wet fall season, however, is correctly reproduced,
466 but with a too early start and plateau. The CDF-t bias correction method is able to correct the
467 annual cycle of precipitation. The dry season is therefore consistent with the reference. In
468 terms of intensity, ALADIN corrected shows an increase in intensity of the wet season peak
469 ($> 0.4 \text{ mm.h}^{-1}$). We do not find this signal with AROME after correction. There is a dry signal
470 for AROME corrected for the summer months. Results show no signal of wet season
471 lengthening between the historical period and the future RCP 8.5 scenario.

472



473
474
475
476
477
478
479
480
481
482

Figure 2: Annual cycle of daily-aggregated minimum and maximum 2m- temperature (Tmin and Tmax) and hourly precipitation for raw (left) and bias-corrected (right) climate datasets. A 30-day rolling mean has been applied in order to smooth the high frequency natural variability.



483 In terms of precipitation distribution, for the evaluation (retrospective) simulations, AROME
484 performs better than ALADIN, especially for the precipitation extremes (Figure 3). The most
485 extreme events (> quantile 99.9) remain underestimated for AROME. (Fumière et al., 2019;
486 Caillaud et al., 2021; Lucas-Picher et al., 2023) have already shown the added value of the
487 AROME CPM compared to its driving RCM, ALADIN, for modeling extreme hourly
488 precipitation. This result confirms these past studies at the scale of a small catchment in the
489 Cévennes region where AROME shows a clear added value (Caillaud et al., 2021).

490
491 The future ALADIN projected rainfall is lower than that of AROME, for the whole distribution.
492 Extreme projected precipitation for ALADIN is lower than for the historical AROME data,
493 partially due to the persistent bias. However, the projected hourly precipitation shows an
494 increase of extreme hourly rainfall (> 95th percentile) under a warmer climate (RCP 8.5
495 projection) for both models. This signal is stronger for the most extreme hourly rainfall (>99.9th
496 percentile) and for the AROME simulation. This local-scale result is in agreement with the
497 broader multi-model ensemble study of Pichelli et al. (2021), which compared an ensemble of
498 CPMs and their driving RCMs over 10-year periods (historical and future). They found a
499 consistent signal of hourly rainfall extremes over southern France between CPMs and RCMs
500 for the wet season (fall). For the dry season, a slight decrease of the 99.9th percentile of hourly
501 precipitation of CPMs is shown, consistent with the annual cycle projection of Figure 2. The
502 large increase of the hourly extreme simulated precipitation is maintained after the bias
503 correction. The signal of the projected precipitation, after bias correction, is largely positive for
504 all probabilities exceeding 95th percentiles for both models. While ALADIN shows a stronger
505 increase for the 95th and 99th percentiles than those of AROME, AROME produces the most
506 positive trend for the most extreme hourly corrected rainfall (see Table 2). Indeed, the most
507 extreme projected hourly rainfall is therefore expected to reach hourly rainfalls that have never
508 been observed at the catchment scale (> 40 mm.h⁻¹).

509
510

Percentile	AROME	ALADIN
95 th	+4.1	+16.6
99 th	+17.5	+36.5
99.9 th	+52.4	+28

511

512 **Table 2: Changes of extreme hourly corrected precipitation (%) under RCP 8.5 scenario**
513 **relative to historical simulation for AROME and ALADIN.**

514

515

516

517

518

519

520

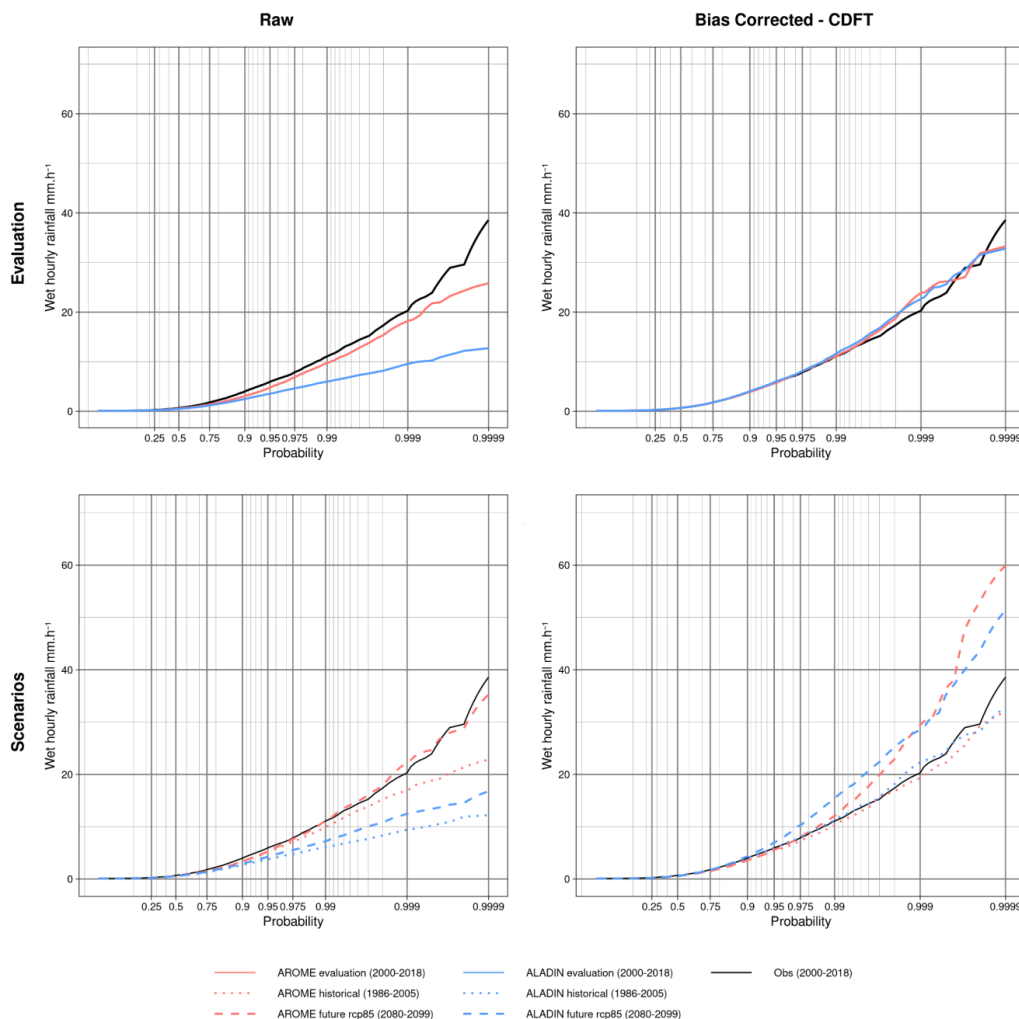
521

522

523



524
 525
 526



527 **Figure 3: Distribution of wet hourly rainfall (> 0.1mm.h⁻¹) for raw (left) and bias-**
 528 **corrected (right) precipitation datasets. The upper panels show the retrospective**
 529 **simulations (2000-2018). The lower panels depict the historical (1986-2005) and future**
 530 **(2080-2099) simulations under the RCP 8.5 scenario. COMEPHORE observed hourly**
 531 **rainfall is appended to all panels (2000-2018). Probabilities under the abscissa are**
 532 **shown under a Gumbel transformation.**
 533
 534
 535



536 4.2. Hydrological modeling to reproduce floods events

537

538 Table 3 presents a summary of the performance metrics of the hydrological models (GR5H
539 and CREST) calculated over the evaluation period. GR5H reproduces well the observed
540 discharge with KGE and NSE scores higher than 0.75 (Table 1). High flows and mean flows
541 are correctly simulated even if they are slightly underestimated. The CREST performance is
542 lower for all the metrics. It shows an acceptable global efficiency and an overestimation of
543 both mean flows and high flows. Both hydrological models underestimate flood peaks.
544

	NSE	KGE	Bias on Mean flows (%)	Bias on Q99.9 (%)	Bias on POT (%)
GR5H	0.76	0.85	-2.28	-3.7	-9.21
CREST	0.54	0.68	8.49	19.9	-19.6

545

546 **Table 3: Evaluation of hydrological models simulations against observed discharge**
547 **(2002-2018). Results for general efficiency scores (NSE: Nash–Sutcliffe efficiency, KGE:**
548 **Kling-Gupta efficiency) and relative biases on mean flows, high flows (quantile 99.9)**
549 **and flood peaks (observed flood peak over threshold).**

550

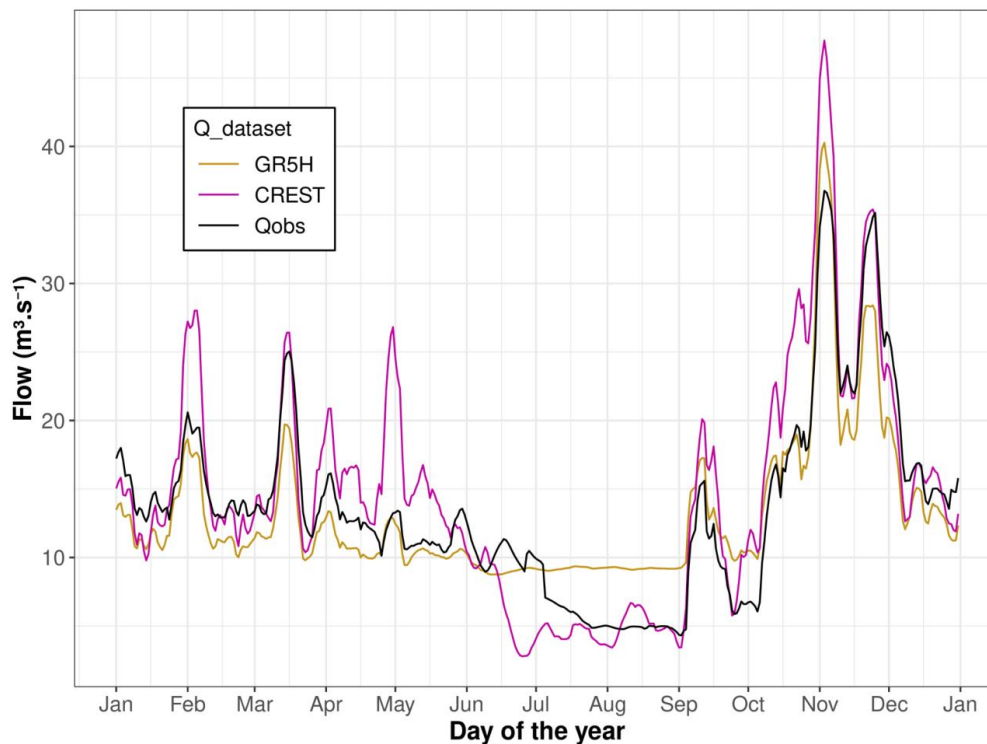
551 Figure 4 shows the annual cycle of discharge at the outlet of the Gardon d'Anduze catchment.
552 Both models are able to reproduce the annual cycle, in particular the high-flow season caused
553 by HPEs and floods events. As seen on Table 3, CREST tends to produce a more excessive
554 discharge response to rainfall than GR5H. GR5H tends to overestimate low flows for summer
555 months, which is however not the focus of the present work. One should keep in mind that the
556 two hydrological models have been calibrated using a different strategy, all parameters of
557 GR5H have been calibrated while most of CREST parameters used a priori estimates, since
558 it is a common strategy for fully distributed physically-based models (Clark et al., 2017).
559

560

561 These results must be moderated looking at Figure 5, which shows the cumulative distribution
562 of the observed discharge along with the GR5H and CREST simulated discharge for the
563 evaluation period. The study indeed focuses on the most intense floods events in this
564 catchment, i.e. flood peak above $265 \text{ m}^3 \cdot \text{s}^{-1}$, leading to two floods per year on average. Biases
565 in CREST simulations (Table 3, Figure 4) are not necessarily reflected in the flood distribution
566 since both models manage to reproduce the observed flood distribution on this small
567 catchment. We can see a slight underestimation of the most intense flood by both hydrological
568 models. The most severe flood corresponds to the major flood event of September 2002, one
569 of the most damaging flash floods recorded in France (Delrieu et al., 2005; Vinet, 2008). Even
570 if the return period of this observed flood exceeds 50 years, this outlier value of the distribution
571 of observed POT has to be carefully interpreted. The peak discharge value of a flood of this
572 magnitude is likely inaccurate because of large uncertainties related to the measurement of
573 the water level, the extrapolation from the rating curve, and possible modifications of river bed
574 topography and flow dynamics (Neppel et al., 2010). However, in terms of flood frequency,
575 the number of POTs differs between the two models. While CREST simulates in average 3.1
floods per year, GR5H is closer to observation with in average 1.5 floods per year.

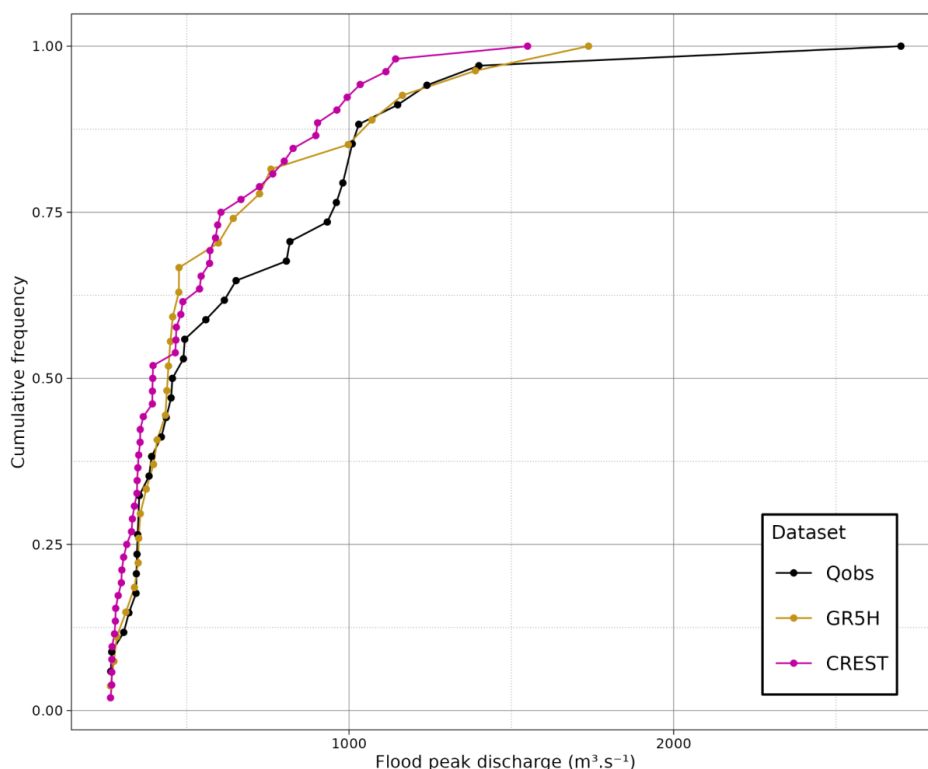


576



577
578
579
580
581
582
583
584
585
586

Figure 4: Annual cycle of discharge for observation, GR5H and CREST evaluation simulations over the 2002-2018 period. Multiyear regime of 8-day averaged flows at Anduze (Gardon d’Anduze catchment)



587
588
589
590
591
592
593
594

Figure 5: Cumulative Distribution Functions (CDFs) of observed and simulated flood peaks over the evaluation period (2002-2018). Both models have been calibrated and run with observed precipitation (COMEPHORE) and PET derived from the observed temperature. The threshold is a fixed discharge value giving two floods per year from the observed discharge ($265 \text{ m}^3 \cdot \text{s}^{-1}$)

595 4.3. Reproducing floods with the climate datasets

596
597
598
599
600
601
602
603
604
605
606
607

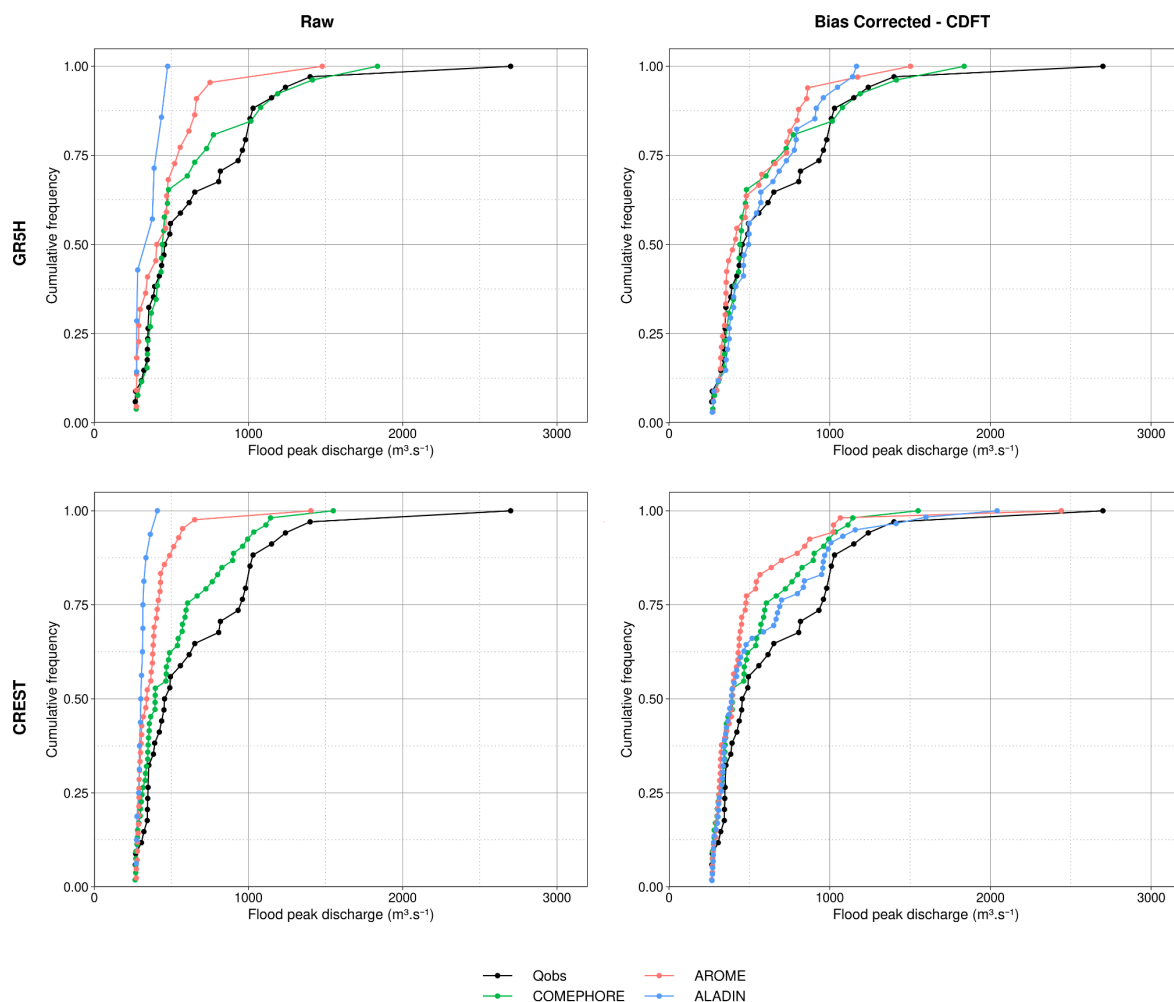
The flood distributions of the AROME- and ALADIN-driven simulations with GR5H and CREST are presented on Figure 6. The AROME and ALADIN datasets are retrospective simulations (evaluation) with (CDFT) and without bias correction. We used the same threshold as in Figure 5, the discharge value ($265 \text{ m}^3 \cdot \text{s}^{-1}$) leading to two observed floods per year after the declustering. First of all, when forced by raw climate simulations, POT distributions are largely underestimated by CREST and GR5H. The hydrological models forced with the AROME CPM reproduce floods intensity better than when forced with ALADIN. This can be observed by the shape of the distributions, which is almost flat for ALADIN. The ALADIN-driven flood distributions fail to reproduce the observed flood frequency with 0.4 and 0.9 floods per year for GR5H and CREST respectively, compared to AROME who simulates an acceptable number of floods (1.2 for GR5H, and 2.3 for CREST). Consequently, AROME seems more



608 reliable than ALADIN in simulating floods with both hydrological models. The results shown in
609 Figure 6 confirm CREST over-reactivity with a higher number of POTs simulated than for
610 GR5H. This model behavior does not impact the flood intensity. Conversely, discharges in the
611 upper half of the flood peak distribution (cumulative frequency > 0.5) are slightly lower for
612 CREST than for GR5H.

613

614 After the CDF-t bias correction, all POT distributions are closer to the hydrological simulation
615 forced by the observed data (green curve). All simulated datasets are compared here with the
616 simulated discharge driven by the observed precipitation (green curve). The ALADIN-driven
617 hydrological simulation shows a slightly better POT distribution than the AROME-driven one
618 for both models, even if the most intense flood event (September 2002) is better simulated
619 with AROME. Bias correction yields an improvement in flood frequency modeling for GR5H
620 with 1.8 floods per year when using the AROME dataset and 1.9 for the ALADIN dataset.
621 However, even after bias-correction, the flood frequency with CREST is higher than the
622 COMEPHORE driven simulation (2.9 and 3.3 floods per year for AROME and ALADIN
623 respectively). To summarize, the added value found for the CPM compared to the RCM in
624 extreme precipitation in previous sections seems to be transmitted for flash flood simulation.
625 Bias correction reduces the difference between climate models, with no remnant bias on POT
626 distribution. The choice of the hydrological model therefore does not seem to impact the
627 results between the forcing climate datasets.



628

629

630 **Figure 6: POT CDF for GR5H (upper panel) and CREST (lower panel) forced by the**

631 **observed and retrospective climate simulations (2001-2018). POT from raw climate**

632 **datasets is on the left and bias-corrected climate datasets on the right. The threshold**

633 **is the same as in Figure 5.**

634

635

636

637

638



639 4.4. Climate change (Flood intensity and frequency)

640

641 This section aims to determine how the flood distribution will evolve in the future for this
642 Mediterranean catchment and whether this evolution is impacted by the different hydrological
643 models and climate models used. Figure 7 is the same as Figure 6, with flood distributions
644 coming only from the hydrological models forced with the AROME and ALADIN climate
645 simulations under the historical and the future RCP 8.5 scenario. In the first place, the two
646 hydrological models show flood peaks discharge weaker for ALADIN than for AROME. CREST
647 simulates higher floods for historical and future projections than GR5H. The shape of the
648 distribution of POT simulated with CREST is less flat than for GR5H distribution, reflecting a
649 behavior similar to a Pareto distribution, hence a tail of the distribution associated with more
650 extreme i.e. rare events. The number of floods is higher for the CREST-driven hydrological
651 simulations than GR5H ones. These simulations can reach a flood frequency exceeding 4
652 floods per year on historical AROME- and ALADIN-driven discharge simulations.

653

654 Flood distributions from the bias-corrected historical and future projections show a good
655 consistency between hydrological models, but higher differences among the climate
656 simulations. Figure 7 highlights a major difference between the AROME CPM and its driving
657 RCM, ALADIN. While the ALADIN-driven simulations indicate for both hydrological models a
658 generalized increase of magnitude of floods, the AROME-driven simulations show a different
659 signal depending on the probability of occurrence. Moderate floods are projected to be weaker
660 in a warmer future when using AROME, but there is a positive increase for the most extreme
661 floods. The threshold related to this change of signal seems to be located between 0.7 and
662 0.75 for both hydrological models, i.e., 25 % to 30 % of the most extreme floods are projected
663 to be stronger in a future climate. Negative changes for CREST are less pronounced than for
664 GR5H, but on the contrary, positive changes above this threshold are stronger, especially for
665 the most extreme projected flood events.

666

667

668

669

670

671

672

673

674

675

676

677

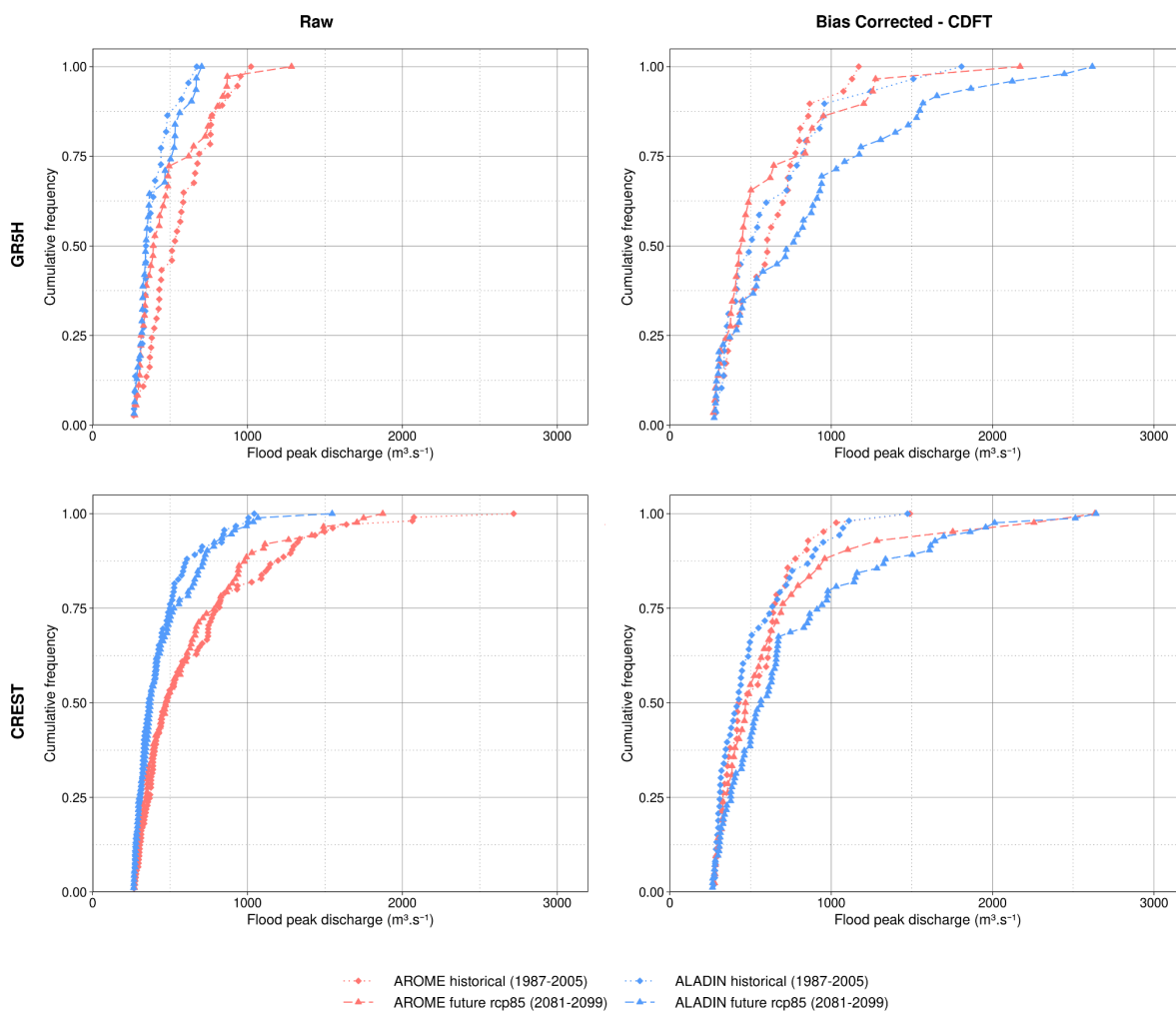
678

679

680

681

682



683
684
685
686
687
688
689
690
691
692
693
694

Figure 7: POT distributions for GR5H (upper panel) and CREST (lower panel) forced by historical and future climate simulations. POTs from raw climate datasets are on the left and those from bias-corrected climate datasets on the right. The threshold is the same as for Figure 5.



695 The different changes in moderate and large floods could be explained by a decrease in future
696 soil moisture, which can compensate for the increase in heavy precipitation for small to
697 moderate floods. This result is in agreement with the studies of Brunner et al. (2021) and
698 Wasko et al. (2023). This is consistent as well with Trambly et al. (2023) and Bertola et al.
699 (2021) who showed the importance of antecedent soil moisture in modulating changes of
700 floods. This threshold behavior is not present for the ALADIN-driven flood simulations. Indeed,
701 the signal for the ALADIN flood projections is positive for almost all the flood distribution,
702 except for the weakest floods where no clear signal is projected. Both bias-corrected ALADIN
703 and AROME flood projection distributions show a strong increasing signal for the distribution
704 tail. ALADIN-driven simulated floods in a future climate reach higher peak values than AROME
705 when simulated by the GR5H model. For CREST, the distribution tail of future floods for
706 AROME and ALADIN are of the same order of magnitude.

707
708 The different behavior between the AROME- and ALADIN-driven flood simulations questions
709 the reliability of low-resolution RCMs for hydrological impact studies related to extreme events.
710 The poor representation of topography along with the parametrization of deep convection for
711 RCMs lead to strong biases on HPE's intensity and temporal distribution. Indeed, extreme
712 rainfall events for ALADIN are generally composed of long-lasting moderate hourly rainfall
713 rather than a more realistic convective precipitation peak. The bias correction method works
714 on each individual hourly time step, but it does not influence the temporal distribution of rainfall
715 events (i.e. hyetograph shape), leading to an over-correction of the HPEs and probably to
716 excessive hydrological reactions (not shown here). This strong bias-correction probably
717 prevents ALADIN from simulating adequately future changes on local processes that are
718 highlighted by the AROME CPM. After bias correction, projected changes in flood frequency
719 also depend on the forcing climate simulation. While AROME shows no change of flood
720 frequency, ALADIN simulates a large increase in the number of floods in future climatic
721 conditions. This trend remains consistent among the two hydrological models, with only little
722 differences between CREST and GR5H simulations (Figure 7).

723
724
725
726
727
728
729
730
731
732
733
734
735
736
737
738
739
740
741



742 4.5. Climate change impact on flood characteristics

743

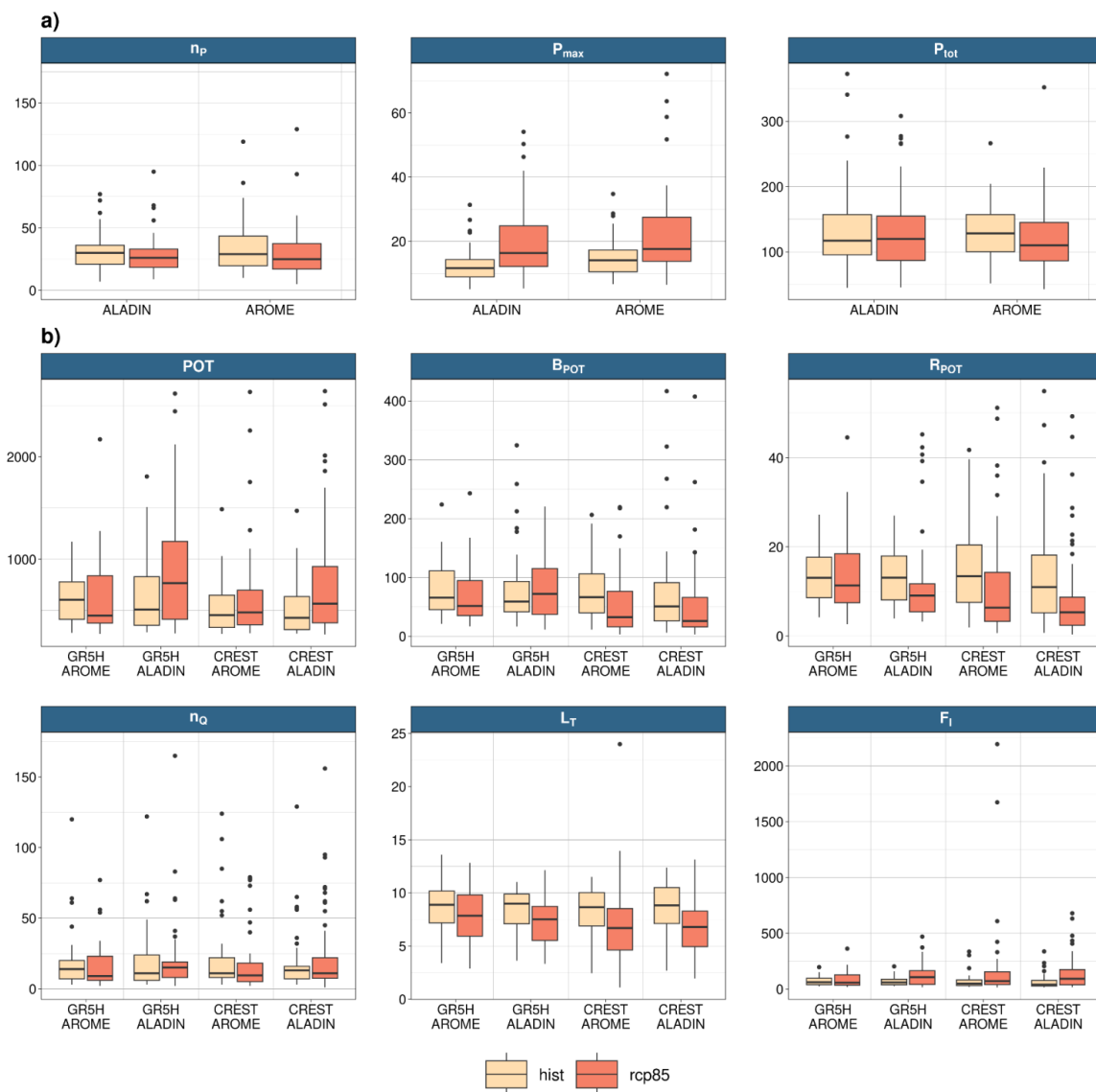
744 Figure 8 shows boxplots of the simulated rainfall events (a)) and flood characteristics produced
745 by these rainfall events (b)) driven by historical and future bias-corrected climate simulations.
746 Every boxplot is made of all values of a specific metric relative to all extracted flood events or
747 the associated rainfall events for one dataset. Firstly, most simulated datasets show a negative
748 future signal for the baseflow component of future floods. Only the GR5H model driven by
749 ALADIN shows a little increase of the median, but this signal is not clear because the
750 distribution becomes wider for future baseflows. The same future positive signal can be found
751 on the ratio metric: all datasets yield a negative trend, reflecting an increase of the runoff part
752 of the streamflow during floods. The maximum hourly precipitation of the largest rainfall event
753 preceding the floods is projected to strongly increase. This result is coherent with Sect. 4.1
754 and confirms that hourly precipitation extremes can yield severe floods in this basin. The most
755 intense increases seem to concern ALADIN-driven simulations with shifts in distribution
756 exceeding 25 % percent (the median in historical simulations corresponds to the first quartile
757 in the future). These results strengthen the confidence of the hypothesis of the decrease of
758 soil moisture leading to the threshold-effect in AROME-forced simulations. In this study, since
759 we do not explicitly simulate soil moisture, the evolution of the baseflow could be linked to soil
760 moisture evolution. The negative trend in the baseflow compensates for the increase of
761 precipitation extremes until a threshold is reached where the most intense hourly rainfall
762 exceeds the infiltration capacity.

763

764 For the ALADIN-driven simulations, the constant increase of POT (Fig. 7, Fig. 8) is a
765 combination of two processes. Firstly, decreases in baseflow are less pronounced for ALADIN
766 than for AROME, in particular for the GR5H hydrological model, reflecting a smaller infiltration
767 capacity, and the prevention of the damping role of soils in a warmer future. Secondly, as
768 explained above, this trend is likely an artifact of the bias-correction causing stronger HPEs in
769 a warmer climate. Indeed, this can be highlighted on Figure 8 where P_{tot} shows a little increase
770 for the ALADIN-driven simulations and a slight decrease in the medians of the AROME rainfall
771 events. Outliers of P_{tot} reach the highest values for the ALADIN-driven simulations. The length
772 of future floods (n_Q) is decreasing for all simulations except for GR5H ALADIN, which shows
773 a slight increase of the median and a lower spread for future scenarios. The lag time (L_T) is
774 projected to decrease for all simulations. This consistent signal of a shorter period between
775 rainfall centroid and flood peak indicates a projected increase of the flood flashiness in this
776 basin (F_I). In more detail, the median of flashiness index, representing reactivity and intensity
777 of floods, is projected to increase for all simulations. The smallest increase of the flashiness
778 index is shown for GR5H-AROME, while the other simulations show noteworthy positive
779 trends and higher spreads. Some outliers reach extremely high values in the future
780 projections, warning of potentially rare, but very extreme flood events occurring in the future.
781 This result is in agreement with the study of Li et al. (2022) who found an increase of flash
782 flood potential over the USA in the high-end emission scenario, notably in southern regions
783 that have a wet convective season such as this Mediterranean catchment.

784

785



786 **Figure 8: Box plots of historical (light orange) and RCP 8.5 future (dark orange) flood**
 787 **events characteristics (b)) and related rainfall events (a) using the bias-corrected**
 788 **simulations. Each characteristic is detailed in Sect. 3.3.**

789
 790
 791
 792



793 Conclusion

794

795 Given the devastating consequences of Mediterranean floods, it is necessary to project if the
796 recent increase in precipitation extremes is going to continue in a warmer climate and have
797 impacts on flood severity. Until now, flood projections are based on regional climate models
798 that cannot accurately simulate precipitation extremes that are yet the main factor causing
799 these floods. In the last 10 years, emerging convection-permitting models using resolutions of
800 a few kilometers show encouraging results in the simulations of short-duration precipitation
801 extremes, opening the door to an enhanced confidence and realism in future flood projections.
802

803

804 This study compared two regional climate model simulations used as inputs of two
805 hydrological models to evaluate the possible climate change impacts on floods in a
806 Mediterranean basin. The AROME convection-permitting climate model (CPM) with a 2.5-km
807 spatial resolution has been compared to the ALADIN model with a 12-km spatial resolution.
808 The evaluation of climate simulations show similar results for both models regarding the
809 reproduction of the annual cycles of temperature and precipitation. There is no added value
810 of using the CPM for the representation of the seasonality of temperature and precipitation.
811 Historical climate simulations are globally too cold with a wet bias for spring and summer.
812 ALADIN and AROME both projected hotter and drier summers in the future, but no drastic
813 changes in the wet season duration and intensity, except a weak increase for ALADIN for the
814 wet season precipitation peak. The added value of the CPM can be clearly seen on rainfall
815 simulation, with a much better representation of extremes with AROME compared to ALADIN,
816 the latter showing a strong underestimation. Both models project an increase in hourly
817 precipitation under the RCP 8.5 scenario. That signal is stronger for events above the 99.9th
818 percentile than more moderate events above the 95th percentile, with a stronger signal for
819 AROME.

819

820 Yet, both climate simulations required a bias-correction to match the observed discharge and
821 notably flood events. Similar simulations, and future scenarios, have been obtained with the
822 two hydrological models considered, a lumped conceptual model, GR5H, and a spatially-
823 distributed, process-based model, CREST, highlighting the robustness of the results given the
824 two different types of model structures. In terms of floods, the hydrological simulations driven
825 by the climate model outputs showed contrasted future discharge, with a general increase of
826 the flood hazard using the ALADIN RCM and on the contrary, an increase only for the largest
827 floods using the AROME CPM. This indicates that the type of climate model can strongly
828 modulate how the increase of extreme rainfall could be translated into changes in flood
829 hazards. The future AROME projections are more in line with previous studies indicating no
830 changes, or a decline of small to moderate floods, caused by a dampening effect due to
831 depleted soil moisture, while the most extreme floods are likely to increase along with the more
832 extreme future rainfall. All simulations also suggest an increase in the flashiness behavior of
833 the basin, with decreased lag times between rainfall and runoff and a larger direct runoff
834 contribution to floods, that could make the flood warning and flood mitigation strategies more
835 difficult in this basin and beyond.

836

837

838 The results of the present study have been obtained with a rather complex, but classic,
839 modeling chain, linking climate models, bias correction and hydrological models. While there



840 are inherent uncertainties in the different steps of the methodology applied herein, the
841 relevance of the results is reinforced since the two hydrological models provided similar
842 conclusions using the same bias-correction method, thus highlighting the differences
843 stemming from the climate simulations. However, there is a clear need to strengthen the
844 conclusions by using a larger ensemble of CPM that are becoming increasingly available for
845 impact studies (Pichelli et al., 2021). Similarly, to reach regionally relevant conclusions and
846 notably to derive adaptation strategies for future flood risks, there is also a need to analyze a
847 broader ensemble of simulated floods on different catchments, and to evaluate how their
848 different areas and properties could modulate floods in a changing climate.
849

850 Code availability

851 The CREST/EF5 software is available at <http://ef5.ou.edu/>, the AirGR package :
852 <https://webgr.inrae.fr/logiciels/airgr/>. SBCK R package is available at
853 <https://github.com/yrobink/SBCK>

854 Data availability

855 Hourly river discharge data could be accessed at: <https://hydro.eaufrance.fr/>, COMEPHORE
856 radar rainfall is available from: <https://radarsmf.aeris-data.fr/>

857 The AROME and ALADIN hourly simulations are available from the corresponding author
858 upon reasonable request.

859 Author contribution

860 NP designed the climate and hydrological experiments and wrote the initial draft. PLP, YT
861 and GT designed the experiments and revised the initial draft. JG, HV contributed to the
862 setup of CREST and revised the manuscript. AA contributed to the data management and
863 revised the manuscript.

864 Competing interests

865 The authors declare that they have no conflict of interest.

866 Financial support

867 This work was supported by the French National Research Agency under the future
868 investment program ANR-18-MPGA-0005.

869 Acknowledgements

870 Thanks are given to the CNRM/MOSCA team for their technical help, in particular to Erwan
871 Brisson, Cecile Caillaud and Edith Cortez.

872



873 References

- 874
875 Addor, N. and Seibert, J.: Bias correction for hydrological impact studies - beyond the daily
876 perspective: INVITED COMMENTARY, *Hydrol. Process.*, 28, 4823–4828,
877 <https://doi.org/10.1002/hyp.10238>, 2014.
878
879 Alfieri, L., Smith, P. J., Thielen-del Pozo, J., and Beven, K. J.: A staggered approach to flash
880 flood forecasting – case study in the Cévennes region, *Adv. Geosci.*, 29, 13–20,
881 <https://doi.org/10.5194/adgeo-29-13-2011>, 2011.
882
883 Alfieri, L., Burek, P., Feyen, L., and Forzieri, G.: Global warming increases the frequency of
884 river floods in Europe, *Hydrol. Earth Syst. Sci.*, 19, 2247–2260, [https://doi.org/10.5194/hess-](https://doi.org/10.5194/hess-19-2247-2015)
885 [19-2247-2015](https://doi.org/10.5194/hess-19-2247-2015), 2015.
886
887 Amponsah, W., Ayrál, P.-A., Boudevillain, B., Bouvier, C., Braud, I., Brunet, P., Delrieu, G.,
888 Didon-Lescot, J.-F., Gaume, E., Lebouc, L., Marchi, L., Marra, F., Morin, E., Nord, G.,
889 Payrastre, O., Zoccatelli, D., and Borga, M.: Integrated high-resolution dataset of high-
890 intensity European and Mediterranean flash floods, *Earth Syst. Sci. Data*, 10, 1783–1794,
891 <https://doi.org/10.5194/essd-10-1783-2018>, 2018.
892
893 Ascott, M. J., Christelis, V., Lapworth, D. J., Macdonald, D. M. J., Tindimugaya, C., Iragena,
894 A., Finney, D., Fitzpatrick, R., Marsham, J. H., and Rowell, D. P.: On the application of
895 rainfall projections from a convection-permitting climate model to lumped catchment models,
896 *J. Hydrol.*, 129097, <https://doi.org/10.1016/j.jhydrol.2023.129097>, 2023.
897
898 Astagneau, P. C., Bourgin, F., Andréassian, V., and Perrin, C.: When does a parsimonious
899 model fail to simulate floods? Learning from the seasonality of model bias, *Hydrol. Sci. J.*,
900 66, 1288–1305, <https://doi.org/10.1080/02626667.2021.1923720>, 2021.
901
902 Ban, N., Caillaud, C., Coppola, E., Pichelli, E., Sobolowski, S., Adinolfi, M., Ahrens, B., Alias,
903 A., Anders, I., Bastin, S., Belušić, D., Berthou, S., Brisson, E., Cardoso, R. M., Chan, S. C.,
904 Christensen, O. B., Fernández, J., Fita, L., Frisius, T., Gašparac, G., Giorgi, F., Goergen, K.,
905 Haugen, J. E., Hodnebrog, Ø., Kartsios, S., Katragkou, E., Kendon, E. J., Keuler, K., Lavin-
906 Gullon, A., Lenderink, G., Leutwyler, D., Lorenz, T., Maraun, D., Mercogliano, P., Milovac, J.,
907 Panitz, H.-J., Raffa, M., Remedio, A. R., Schär, C., Soares, P. M. M., Srnec, L., Steensen, B.
908 M., Stocchi, P., Tölle, M. H., Truhetz, H., Vergara-Temprado, J., de Vries, H., Warrach-Sagi,
909 K., Wulfmeyer, V., and Zander, M. J.: The first multi-model ensemble of regional climate
910 simulations at kilometer-scale resolution, part I: evaluation of precipitation, *Clim. Dyn.*, 57,
911 275–302, <https://doi.org/10.1007/s00382-021-05708-w>, 2021.
912
913 Bertola, M., Viglione, A., Vorogushyn, S., Lun, D., Merz, B., and Blöschl, G.: Do small and
914 large floods have the same drivers of change? A regional attribution analysis in Europe,
915 *Hydrol. Earth Syst. Sci.*, 25, 1347–1364, <https://doi.org/10.5194/hess-25-1347-2021>, 2021.
916
917 Blöschl, G., Hall, J., Viglione, A., Perdigão, R. A. P., Parajka, J., Merz, B., Lun, D., Arheimer,
918 B., Aronica, G. T., Bilbashi, A., Boháč, M., Bonacci, O., Borga, M., Čanjevac, I., Castellarin,
919 A., Chirico, G. B., Claps, P., Frolova, N., Ganora, D., Gorbachova, L., Gül, A., Hannaford, J.,
920 Harrigan, S., Kireeva, M., Kiss, A., Kjeldsen, T. R., Kohnová, S., Koskela, J. J., Ledvinka, O.,
921 Macdonald, N., Mavrova-Guirguinova, M., Mediero, L., Merz, R., Molnar, P., Montanari, A.,
922 Murphy, C., Osuch, M., Ovcharuk, V., Radevski, I., Salinas, J. L., Sauquet, E., Šraj, M.,
923 Szolgay, J., Volpi, E., Wilson, D., Zaimi, K., and Živković, N.: Changing climate both
924 increases and decreases European river floods, *Nature*, 573, 108–111,
925 <https://doi.org/10.1038/s41586-019-1495-6>, 2019.



- 927
928 Boé, J., Terray, L., Habets, F., and Martin, E.: Statistical and dynamical downscaling of the
929 Seine basin climate for hydro-meteorological studies, *Int. J. Climatol.*, 27, 1643–1655,
930 <https://doi.org/10.1002/joc.1602>, 2007.
- 931
932 Boudou, M., Lang, M., Vinet, F., and Cœur, D.: Comparative hazard analysis of processes
933 leading to remarkable flash floods (France, 1930–1999), *J. Hydrol.*, 541, 533–552,
934 <https://doi.org/10.1016/j.jhydrol.2016.05.032>, 2016.
- 935
936 Brunner, M. I., Swain, D. L., Wood, R. R., Willkofer, F., Done, J. M., Gilleland, E., and
937 Ludwig, R.: An extremeness threshold determines the regional response of floods to
938 changes in rainfall extremes, *Commun. Earth Environ.*, 2, 173,
939 <https://doi.org/10.1038/s43247-021-00248-x>, 2021.
- 940
941 Caillaud, C., Somot, S., Alias, A., Bernard-Bouissières, I., Fumière, Q., Laurantin, O., Seity,
942 Y., and Ducrocq, V.: Modelling Mediterranean heavy precipitation events at climate scale: an
943 object-oriented evaluation of the CNRM-AROME convection-permitting regional climate
944 model, *Clim. Dyn.*, 56, 1717–1752, <https://doi.org/10.1007/s00382-020-05558-y>, 2021.
- 945
946 Caldas-Alvarez, A., Feldmann, H., Lucio-Eceiza, E., and Pinto, J. G.: Scale-dependency of
947 extreme precipitation processes in regional climate simulations of the greater Alpine region,
948 *Weather Clim. Dyn. Discuss.*, 1–37, <https://doi.org/10.5194/wcd-2022-11>, 2022.
- 949
950 Caumont, O., Mandement, M., Bouttier, F., Eeckman, J., Lebeaupin Brossier, C., Lovat, A.,
951 Nuisser, O., and Laurantin, O.: The heavy precipitation event of 14–15 October 2018 in the
952 Aude catchment: a meteorological study based on operational numerical weather prediction
953 systems and standard and personal observations, *Nat. Hazards Earth Syst. Sci.*, 21, 1135–
954 1157, <https://doi.org/10.5194/nhess-21-1135-2021>, 2021.
- 955
956 Chauveau, M., Chazot, S., Perrin, C., Bourgin, P.-Y., Sauquet, E., Vidal, J.-P., Rouchy, N.,
957 Martin, E., David, J., Norotte, T., Maugis, P., and De Lacaze, X.: Quels impacts des
958 changements climatiques sur les eaux de surface en France à l’horizon 2070 ?, *Houille*
959 *Blanche*, 99, 5–15, <https://doi.org/10.1051/lhb/2013027>, 2013.
- 960
961 Clark, R. A., Flamig, Z. L., Vergara, H., Hong, Y., Gourley, J. J., Mandl, D. J., Frye, S.,
962 Handy, M., and Patterson, M.: Hydrological Modeling and Capacity Building in the Republic
963 of Namibia, *Bull. Am. Meteorol. Soc.*, 98, 1697–1715, <https://doi.org/10.1175/BAMS-D-15-00130.1>, 2017.
- 964
965
966 Coppola, E., Sobolowski, S., Pichelli, E., Raffaele, F., Ahrens, B., Anders, I., Ban, N., Bastin,
967 S., Belda, M., Belusic, D., Caldas-Alvarez, A., Cardoso, R. M., Davolio, S., Dobler, A.,
968 Fernandez, J., Fita, L., Fumiere, Q., Giorgi, F., Goergen, K., Güttler, I., Halenka, T.,
969 Heinzeller, D., Hodnebrog, Ø., Jacob, D., Kartsios, S., Katragkou, E., Kendon, E., Khodayar,
970 S., Kunstmann, H., Knist, S., Lavín-Gullón, A., Lind, P., Lorenz, T., Maraun, D., Marelle, L.,
971 van Meijgaard, E., Milovac, J., Myhre, G., Panitz, H.-J., Piazza, M., Raffa, M., Raub, T.,
972 Rockel, B., Schär, C., Sieck, K., Soares, P. M. M., Somot, S., Srnec, L., Stocchi, P., Tölle, M.
973 H., Truhetz, H., Vautard, R., de Vries, H., and Warrach-Sagi, K.: A first-of-its-kind multi-
974 model convection permitting ensemble for investigating convective phenomena over Europe
975 and the Mediterranean, *Clim. Dyn.*, 55, 3–34, <https://doi.org/10.1007/s00382-018-4521-8>,
976 2020.
- 977
978 Coron, L., Thirel, G., Delaigue, O., Perrin, C., and Andréassian, V.: The suite of lumped GR
979 hydrological models in an R package, *Environ. Model. Softw.*, 94, 166–171,
980 <https://doi.org/10.1016/j.envsoft.2017.05.002>, 2017.
- 981



- 982 Coron, L., Delaigue, O., Thirel, G., Dorchies, D., Perrin, C., and Michel, C.: airGR: Suite of
983 GR Hydrological Models for Precipitation-Runoff Modelling. R package version 1.7.4.,
984 <https://doi.org/10.15454/EX11NA>, 2020.
- 985
986 Cunnane, C.: A particular comparison of annual maxima and partial duration series methods
987 of flood frequency prediction, *J. Hydrol.*, 18, 257–271, [https://doi.org/10.1016/0022-1694\(73\)90051-6](https://doi.org/10.1016/0022-1694(73)90051-6), 1973.
- 988
989
990 Dankers, R. and Feyen, L.: Flood hazard in Europe in an ensemble of regional climate
991 scenarios, *J. Geophys. Res. Atmospheres*, 114, <https://doi.org/10.1029/2008JD011523>,
992 2009.
- 993
994 Dee, D. P., Uppala, S. M., Simmons, A. J., Berrisford, P., Poli, P., Kobayashi, S., Andrae, U.,
995 Balmaseda, M. A., Balsamo, G., Bauer, P., Bechtold, P., Beljaars, A. C. M., van de Berg, L.,
996 Bidlot, J., Bormann, N., Delsol, C., Dragani, R., Fuentes, M., Geer, A. J., Haimberger, L.,
997 Healy, S. B., Hersbach, H., Hólm, E. V., Isaksen, L., Kållberg, P., Köhler, M., Matricardi, M.,
998 McNally, A. P., Monge-Sanz, B. M., Morcrette, J.-J., Park, B.-K., Peubey, C., de Rosnay, P.,
999 Tavolato, C., Thépaut, J.-N., and Vitart, F.: The ERA-Interim reanalysis: configuration and
1000 performance of the data assimilation system, *Q. J. R. Meteorol. Soc.*, 137, 553–597,
1001 <https://doi.org/10.1002/qj.828>, 2011.
- 1002
1003 Delrieu, G., Nicol, J., Yates, E., Kirstetter, P.-E., Creutin, J.-D., Anquetin, S., Obled, C.,
1004 Saulnier, G.-M., Ducrocq, V., Gaume, E., Payrastra, O., Andrieu, H., Ayrat, P.-A., Bouvier,
1005 C., Neppel, L., Livet, M., Lang, M., du-Châtelet, J. P., Walpersdorf, A., and Wobrock, W.:
1006 The Catastrophic Flash-Flood Event of 8–9 September 2002 in the Gard Region, France: A
1007 First Case Study for the Cévennes–Vivarais Mediterranean Hydrometeorological
1008 Observatory, *J. Hydrometeorol.*, 6, 34–52, <https://doi.org/10.1175/JHM-400.1>, 2005.
- 1009
1010 Ficchi, A., Perrin, C., and Andréassian, V.: Hydrological modelling at multiple sub-daily time
1011 steps: Model improvement via flux-matching, *J. Hydrol.*, 575, 1308–1327,
1012 <https://doi.org/10.1016/j.jhydrol.2019.05.084>, 2019.
- 1013
1014 Flamig, Z. L., Vergara, H., and Gourley, J. J.: The Ensemble Framework For Flash Flood
1015 Forecasting (EF5) v1.2: description and case study, *Geosci. Model Dev.*, 13, 4943–4958,
1016 <https://doi.org/10.5194/gmd-13-4943-2020>, 2020.
- 1017
1018 Fumière, Q., Somot, S., Caillaud, C., and Alias, A.: Climate change and heavy precipitation
1019 events in South-Eastern France., in: *Geophysical Research Abstracts*, 2019.
- 1020 Fumière, Q., Déqué, M., Nuissier, O., Somot, S., Alias, A., Caillaud, C., Laurantin, O., and
1021 Seity, Y.: Extreme rainfall in Mediterranean France during the fall: added value of the
1022 CNRM-AROME Convection-Permitting Regional Climate Model, *Clim. Dyn.*, 55, 77–91,
1023 <https://doi.org/10.1007/s00382-019-04898-8>, 2020.
- 1024
1025 Giorgi, F.: Thirty Years of Regional Climate Modeling: Where Are We and Where Are We
1026 Going next?, *J. Geophys. Res. Atmospheres*, 124, 5696–5723,
1027 <https://doi.org/10.1029/2018JD030094>, 2019.
- 1028
1029 Giorgi, F. and Gutowski, W. J.: Regional Dynamical Downscaling and the CORDEX
1030 Initiative, *Annu. Rev. Environ. Resour.*, 40, 467–490, <https://doi.org/10.1146/annurev-environ-102014-021217>, 2015.
- 1031
1032
1033 Gupta, H. V., Kling, H., Yilmaz, K. K., and Martinez, G. F.: Decomposition of the mean
1034 squared error and NSE performance criteria: Implications for improving hydrological
1035 modelling, *J. Hydrol.*, 377, 80–91, <https://doi.org/10.1016/j.jhydrol.2009.08.003>, 2009.
- 1036 Hargreaves, G. H. and Samani, Z. A.: Estimating Potential Evapotranspiration, *J. Irrig. Drain.*



- 1037 Div., 108, 225–230, <https://doi.org/10.1061/JRCEA4.0001390>, 1982.
1038
1039 Huang, S., Krysanova, V., and Hattermann, F. F.: Does bias correction increase reliability of
1040 flood projections under climate change? A case study of large rivers in Germany, *Int. J.*
1041 *Climatol.*, 34, 3780–3800, <https://doi.org/10.1002/joc.3945>, 2014.
1042 J. A. Vrugt, C. J.F. ter Braak, C. G.H. Diks, B. A. Robinson, J. M. Hyman, and D. Higdon:
1043 Accelerating Markov Chain Monte Carlo Simulation by Differential Evolution with Self-
1044 Adaptive Randomized Subspace Sampling, *Int. J. Nonlinear Sci. Numer. Simul.*, 10, 273–
1045 290, <https://doi.org/10.1515/IJNSNS.2009.10.3.273>, 2009.
1046
1047 Kay, A.: Differences in hydrological impacts using regional climate model and nested
1048 convection-permitting model data, *Clim. Change*, 173, 11, [https://doi.org/10.1007/s10584-](https://doi.org/10.1007/s10584-022-03405-z)
1049 [022-03405-z](https://doi.org/10.1007/s10584-022-03405-z), 2022.
1050
1051 Kay, A. L., Reynard, N. S., and Jones, R. G.: RCM rainfall for UK flood frequency estimation.
1052 I. Method and validation, *J. Hydrol.*, 318, 151–162,
1053 <https://doi.org/10.1016/j.jhydrol.2005.06.012>, 2006.
1054
1055 Kay, A. L., Rudd, A. C., Davies, H. N., Kendon, E. J., and Jones, R. G.: Use of very high
1056 resolution climate model data for hydrological modelling: baseline performance and future
1057 flood changes, *Clim. Change*, 133, 193–208, <https://doi.org/10.1007/s10584-015-1455-6>,
1058 2015.
1059
1060 Khodayar, S., Fosser, G., Berthou, S., Davolio, S., Drobinski, P., Ducrocq, V., Ferretti, R.,
1061 Nuret, M., Pichelli, E., Richard, E., and Bock, O.: A seamless weather–climate multi-model
1062 intercomparison on the representation of a high impact weather event in the western
1063 Mediterranean: HyMeX IOP12, *Q. J. R. Meteorol. Soc.*, 142, 433–452,
1064 <https://doi.org/10.1002/qj.2700>, 2016.
1065
1066 Khodayar, S., Kalthoff, N., and Kottmeier, C.: Atmospheric conditions associated with heavy
1067 precipitation events in comparison to seasonal means in the western mediterranean region,
1068 *Clim. Dyn.*, 51, 951–967, <https://doi.org/10.1007/s00382-016-3058-y>, 2018.
1069 Köplin, N., Schädler, B., Viviroli, D., and Weingartner, R.: Seasonality and magnitude of
1070 floods in Switzerland under future climate change, *Hydrol. Process.*, 28, 2567–2578,
1071 <https://doi.org/10.1002/hyp.9757>, 2014.
1072
1073 Lang, M., Ouarda, T. B. M. J., and Bobée, B.: Towards operational guidelines for over-
1074 threshold modeling, *J. Hydrol.*, 225, 103–117, [https://doi.org/10.1016/S0022-1694\(99\)00167-](https://doi.org/10.1016/S0022-1694(99)00167-5)
1075 [5](https://doi.org/10.1016/S0022-1694(99)00167-5), 1999.
1076
1077 Laurantin, O., Tabary, P., Dupuy, P., L’Henaff, G., Merlier, C., and Soubeyroux, J.-M.: A 10-
1078 year (1997–2006) reanalysis of quantitative precipitation estimation over France, in: 7th
1079 European conference on radar in meteorology and hydrology, 1–5, 2012.
1080 Lemaitre-Basset, T., Collet, L., Thirel, G., Parajka, J., Evin, G., and Hingray, B.: Climate
1081 change impact and uncertainty analysis on hydrological extremes in a French Mediterranean
1082 catchment, *Hydrol. Sci. J.*, 66, 888–903, <https://doi.org/10.1080/02626667.2021.1895437>,
1083 2021.
1084
1085 Li, Z., Chen, M., Gao, S., Luo, X., Gourley, J. J., Kirstetter, P., Yang, T., Kolar, R.,
1086 McGovern, A., Wen, Y., Rao, B., Yami, T., and Hong, Y.: CREST-iMAP v1.0: A fully coupled
1087 hydrologic-hydraulic modeling framework dedicated to flood inundation mapping and
1088 prediction, *Environ. Model. Softw.*, 141, 105051,
1089 <https://doi.org/10.1016/j.envsoft.2021.105051>, 2021.
1090
1091 Li, Z., Gao, S., Chen, M., Gourley, J. J., and Hong, Y.: Spatiotemporal Characteristics of US



- 1092 Floods: Current Status and Forecast Under a Future Warmer Climate, *Earths Future*, 10,
1093 e2022EF002700, <https://doi.org/10.1029/2022EF002700>, 2022a.
1094
1095
1096
1097 Li, Z., Gao, S., Chen, M., Gourley, J. J., Liu, C., Prein, A. F., and Hong, Y.: The
1098 conterminous United States are projected to become more prone to flash floods in a high-
1099 end emissions scenario, *Commun. Earth Environ.*, 3, 86, <https://doi.org/10.1038/s43247-022-00409-6>, 2022b.
1100
1101
1102 Lobligeois, F.: Mieux connaitre la distribution spatiale des pluies améliore-t-il la modélisation
1103 des crues? Diagnostic sur 181 bassins versants français, 313, 2014.
1104
1105 Lucas-Picher, P., Argüeso, D., Brisson, E., Trambly, Y., Berg, P., Lemonsu, A., Kotlarski,
1106 S., and Caillaud, C.: Convection-permitting modeling with regional climate models: Latest
1107 developments and next steps, *WIREs Clim. Change*, 12, e731,
1108 <https://doi.org/10.1002/wcc.731>, 2021.
1109
1110 Lucas-Picher, P., Brisson, E., Caillaud, C., Alias, A., Nabat, P., Lemonsu, A., Poncet, N.,
1111 Cortés Hernandez, V. E., Michau, Y., Doury, A., Monteiro, D., and Somot, S.: Evaluation of
1112 the convection-permitting regional climate model CNRM-AROME41t1 over Northwestern
1113 Europe, *Clim. Dyn.*, <https://doi.org/10.1007/s00382-022-06637-y>, 2023.
1114
1115 Maraun, D.: Bias Correcting Climate Change Simulations - a Critical Review, *Curr. Clim.*
1116 *Change Rep.*, 2, 211–220, <https://doi.org/10.1007/s40641-016-0050-x>, 2016.
1117 Maurer, E. P., Brekke, L., Pruitt, T., and Duffy, P. B.: Fine-resolution climate projections
1118 enhance regional climate change impact studies, *Eos Trans. Am. Geophys. Union*, 88, 504–
1119 504, <https://doi.org/10.1029/2007EO470006>, 2007.
1120
1121 Mendoza, P. A., Mizukami, N., Ikeda, K., Clark, M. P., Gutmann, E. D., Arnold, J. R., Brekke,
1122 L. D., and Rajagopalan, B.: Effects of different regional climate model resolution and forcing
1123 scales on projected hydrologic changes, *J. Hydrol.*, 541, 1003–1019,
1124 <https://doi.org/10.1016/j.jhydrol.2016.08.010>, 2016.
1125
1126 Michelangeli, P.-A., Vrac, M., and Loukos, H.: Probabilistic downscaling approaches:
1127 Application to wind cumulative distribution functions, *Geophys. Res. Lett.*, 36,
1128 <https://doi.org/10.1029/2009GL038401>, 2009.
1129
1130 Moussa, R.: When monstrosity can be beautiful while normality can be ugly: assessing the
1131 performance of event-based flood models, *Hydrol. Sci. J.*, 55, 1074–1084,
1132 <https://doi.org/10.1080/02626667.2010.505893>, 2010.
1133
1134 Nabat, P., Somot, S., Cassou, C., Mallet, M., Michou, M., Bouniol, D., Decharme, B., Drugé,
1135 T., Roehrig, R., and Saint-Martin, D.: Modulation of radiative aerosols effects by atmospheric
1136 circulation over the Euro-Mediterranean region, *Atmospheric Chem. Phys.*, 20, 8315–8349,
1137 <https://doi.org/10.5194/acp-20-8315-2020>, 2020.
1138
1139 Nash, J. E. and Sutcliffe, J. V.: River flow forecasting through conceptual models part I — A
1140 discussion of principles, *J. Hydrol.*, 10, 282–290, [https://doi.org/10.1016/0022-1694\(70\)90255-6](https://doi.org/10.1016/0022-1694(70)90255-6), 1970.
1141
1142
1143 Neppel, L., Renard, B., Lang, M., Ayrat, P.-A., Coeur, D., Gaume, E., Jacob, N., Payrastre,
1144 O., Pobanz, K., and Vinet, F.: Flood frequency analysis using historical data: accounting for
1145 random and systematic errors, *Hydrol. Sci. Journal–Journal Sci. Hydrol.*, 55, 192–208, 2010.
1146 Nuissier, O., Joly, B., Joly, A., Ducrocq, V., and Arbogast, P.: A statistical downscaling to



- 1147 identify the large-scale circulation patterns associated with heavy precipitation events over
1148 southern France, *Q. J. R. Meteorol. Soc.*, 137, 1812–1827, <https://doi.org/10.1002/qj.866>,
1149 2011.
1150
1151
1152 Oudin, L., Hervieu, F., Michel, C., Perrin, C., Andréassian, V., Anctil, F., and Loumagne, C.:
1153 Which potential evapotranspiration input for a lumped rainfall–runoff model?, *J. Hydrol.*, 303,
1154 290–306, <https://doi.org/10.1016/j.jhydrol.2004.08.026>, 2005.
1155
1156 Pichelli, E., Coppola, E., Sobolowski, S., Ban, N., Giorgi, F., Stocchi, P., Alias, A., Belušić,
1157 D., Berthou, S., Caillaud, C., Cardoso, R. M., Chan, S., Christensen, O. B., Dobler, A., de
1158 Vries, H., Goergen, K., Kendon, E. J., Keuler, K., Lenderink, G., Lorenz, T., Mishra, A. N.,
1159 Panitz, H.-J., Schär, C., Soares, P. M. M., Truhetz, H., and Vergara-Temprado, J.: The first
1160 multi-model ensemble of regional climate simulations at kilometer-scale resolution part 2:
1161 historical and future simulations of precipitation, *Clim. Dyn.*, 56, 3581–3602,
1162 <https://doi.org/10.1007/s00382-021-05657-4>, 2021.
1163
1164 Prein, A. F., Langhans, W., Fosser, G., Ferrone, A., Ban, N., Goergen, K., Keller, M., Tölle,
1165 M., Gutjahr, O., Feser, F., Brisson, E., Kollet, S., Schmidli, J., Lipzig, N. P. M., and Leung,
1166 R.: A review on regional convection-permitting climate modeling: Demonstrations, prospects,
1167 and challenges, *Rev. Geophys.*, 53, 323–361, <https://doi.org/10.1002/2014RG000475>, 2015.
1168 Prein, A. F., Gobiet, A., Truhetz, H., Keuler, K., Goergen, K., Teichmann, C., Fox Maule, C.,
1169 van Meijgaard, E., Déqué, M., Nikulin, G., Vautard, R., Colette, A., Kjellström, E., and Jacob,
1170 D.: Precipitation in the EURO-CORDEX 0.11° and 0.44° simulations:
1171 high resolution, high benefits?, *Clim. Dyn.*, 46, 383–412, [https://doi.org/10.1007/s00382-015-](https://doi.org/10.1007/s00382-015-2589-y)
1172 2589-y, 2016.
1173
1174 Quintero, F., Villarini, G., Prein, A. F., Krajewski, W. F., and Zhang, W.: On the Role of
1175 Atmospheric Simulations Horizontal Grid Spacing for Flood Modeling, In Review,
1176 <https://doi.org/10.21203/rs.3.rs-821389/v1>, 2021.
1177
1178 Reszler, C., Switanek, M. B., and Truhetz, H.: Convection-permitting regional climate
1179 simulations for representing floods in small- and medium-sized catchments in the Eastern
1180 Alps, *Nat. Hazards Earth Syst. Sci.*, 18, 2653–2674, [https://doi.org/10.5194/nhess-18-2653-](https://doi.org/10.5194/nhess-18-2653-2018)
1181 2018, 2018.
1182
1183 Ribes, A., Thao, S., Vautard, R., Dubuisson, B., Somot, S., Colin, J., Planton, S., and
1184 Soubeyrou, J.-M.: Observed increase in extreme daily rainfall in the French Mediterranean,
1185 *Clim. Dyn.*, 52, 1095–1114, <https://doi.org/10.1007/s00382-018-4179-2>, 2019.
1186 Ricard, D., Ducrocq, V., and Auger, L.: A Climatology of the Mesoscale Environment
1187 Associated with Heavily Precipitating Events over a Northwestern Mediterranean Area, *J.*
1188 *Appl. Meteorol. Climatol.*, 51, 468–488, <https://doi.org/10.1175/JAMC-D-11-017.1>, 2012.
1189 Robin, Y.: SBCK: Statistical Bias Correction Kit, 2022.
1190
1191 Rojas, R., Feyen, L., Dosio, A., and Bavera, D.: Improving pan-European hydrological
1192 simulation of extreme events through statistical bias correction of RCM-driven climate
1193 simulations, *Hydrol. Earth Syst. Sci.*, 15, 2599–2620, [https://doi.org/10.5194/hess-15-2599-](https://doi.org/10.5194/hess-15-2599-2011)
1194 2011, 2011.
1195
1196 Roux, H., Labat, D., Garambois, P.-A., Maubourguet, M.-M., Chorda, J., and Dartus, D.: A
1197 physically-based parsimonious hydrological model for flash floods in Mediterranean
1198 catchments, *Nat. Hazards Earth Syst. Sci.*, 11, 2567–2582, [https://doi.org/10.5194/nhess-](https://doi.org/10.5194/nhess-11-2567-2011)
1199 11-2567-2011, 2011.
1200
1201 Rummukainen, M.: State-of-the-art with regional climate models, *WIREs Clim. Change*, 1,



- 1202 82–96, <https://doi.org/10.1002/wcc.8>, 2010.
1203
1204 Sharma, A., Wasko, C., and Lettenmaier, D. P.: If Precipitation Extremes Are Increasing,
1205 Why Aren't Floods?, *Water Resour. Res.*, 54, 8545–8551,
1206 <https://doi.org/10.1029/2018WR023749>, 2018.
1207 Teutschbein, C. and Seibert, J.: Regional Climate Models for Hydrological Impact Studies at
1208 the Catchment Scale: A Review of Recent Modeling Strategies, *Geogr. Compass*, 4, 834–
1209 860, <https://doi.org/10.1111/j.1749-8198.2010.00357.x>, 2010.
1210
1211 Teutschbein, C. and Seibert, J.: Bias correction of regional climate model simulations for
1212 hydrological climate-change impact studies: Review and evaluation of different methods, *J.*
1213 *Hydrol.*, 456–457, 12–29, <https://doi.org/10.1016/j.jhydrol.2012.05.052>, 2012.
1214
1215 Thober, S., Kumar, R., Wanders, N., Marx, A., Pan, M., Rakovec, O., Samaniego, L.,
1216 Sheffield, J., Wood, E. F., and Zink, M.: Multi-model ensemble projections of European river
1217 floods and high flows at 1.5, 2, and 3 degrees global warming, *Environ. Res. Lett.*, 13,
1218 014003, <https://doi.org/10.1088/1748-9326/aa9e35>, 2018.
1219
1220 Toukourou, M., Johannet, A., Dreyfus, G., and Ayrat, P.-A.: Rainfall-runoff modeling of flash
1221 floods in the absence of rainfall forecasts: the case of “Cévenol flash floods,” *Appl. Intell.*, 35,
1222 178–189, <https://doi.org/10.1007/s10489-010-0210-y>, 2011.
1223
1224 Trambly, Y. and Somot, S.: Future evolution of extreme precipitation in the Mediterranean,
1225 *Clim. Change*, 151, 289–302, <https://doi.org/10.1007/s10584-018-2300-5>, 2018.
1226
1227 Trambly, Y., Mimeau, L., Neppel, L., Vinet, F., and Sauquet, E.: Detection and attribution of
1228 flood trends in Mediterranean basins, *Hydrol. Earth Syst. Sci.*, 23, 4419–4431,
1229 <https://doi.org/10.5194/hess-23-4419-2019>, 2019.
1230
1231 Trambly, Y., Arnaud, P., Artigue, G., Lang, M., Paquet, E., Neppel, L., and Sauquet, E.:
1232 Changes in Mediterranean flood processes and seasonality, *Hydrol. Earth Syst. Sci.*
1233 *Discuss.*, 1–25, <https://doi.org/10.5194/hess-2023-46>, 2023.
1234
1235 Vannier, O., Braud, I., and Anquetin, S.: Regional estimation of catchment-scale soil
1236 properties by means of streamflow recession analysis for use in distributed hydrological
1237 models, *Hydrol. Process.*, 28, 6276–6291, <https://doi.org/10.1002/hyp.10101>, 2014.
1238
1239 Vautard, R., Kadyrov, N., Iles, C., Boberg, F., Buonomo, E., Bülow, K., Coppola, E., Corre,
1240 L., van Meijgaard, E., Nogherotto, R., Sandstad, M., Schwingshackl, C., Somot, S., Aalbers,
1241 E., Christensen, O. B., Ciarlo, J. M., Demory, M.-E., Giorgi, F., Jacob, D., Jones, R. G.,
1242 Keuler, K., Kjellström, E., Lenderink, G., Levvasseur, G., Nikulin, G., Sillmann, J., Solidoro,
1243 C., Sørland, S. L., Steger, C., Teichmann, C., Warrach-Sagi, K., and Wulfmeyer, V.:
1244 Evaluation of the Large EURO-CORDEX Regional Climate Model Ensemble, *J. Geophys.*
1245 *Res. Atmospheres*, 126, e2019JD032344, <https://doi.org/10.1029/2019JD032344>, 2021.
1246
1247 Vinet, F.: Geographical analysis of damage due to flash floods in southern France: The
1248 cases of 12–13 November 1999 and 8–9 September 2002, *Appl. Geogr.*, 28, 323–336,
1249 <https://doi.org/10.1016/j.apgeog.2008.02.007>, 2008.
1250
1251 Vinet, F., Cherel, J.-P., Weiss, K., Lewandowski, M., and Boissier, L.: Flood related mortality
1252 in the French Mediterranean region (1980–2020), *LHB*, 108, 2097022,
1253 <https://doi.org/10.1080/27678490.2022.2097022>, 2022.
1254
1255 Voltaire, A., Sanchez-Gomez, E., Salas y Mélia, D., Decharme, B., Cassou, C., Sénési, S.,
1256 Valcke, S., Beau, I., Alias, A., Chevallier, M., Déqué, M., Deshayes, J., Douville, H.,



- 1257 Fernandez, E., Madec, G., Maisonnave, E., Moine, M.-P., Planton, S., Saint-Martin, D.,
1258 Szopa, S., Tyteca, S., Alkama, R., Belamari, S., Braun, A., Coquart, L., and Chauvin, F.: The
1259 CNRM-CM5.1 global climate model: description and basic evaluation, *Clim. Dyn.*, 40, 2091–
1260 2121, <https://doi.org/10.1007/s00382-011-1259-y>, 2013.
1261
1262
1263 Vrac, M., Drobinski, P., Merlo, A., Herrmann, M., Lavaysse, C., Li, L., and Somot, S.:
1264 Dynamical and statistical downscaling of the French Mediterranean climate: uncertainty
1265 assessment, *Nat. Hazards Earth Syst. Sci.*, 12, 2769–2784, <https://doi.org/10.5194/nhess-12-2769-2012>, 2012.
1266
1267
1268 Vrac, M., Noël, T., and Vautard, R.: Bias correction of precipitation through Singularity
1269 Stochastic Removal: Because occurrences matter, *J. Geophys. Res. Atmospheres*, 121,
1270 5237–5258, <https://doi.org/10.1002/2015JD024511>, 2016.
1271
1272 Wang, J., Hong, Y., Li, L., Gourley, J. J., Khan, S. I., Yilmaz, K. K., Adler, R. F., Policelli, F.,
1273 S., Habib, S., Irwn, D., Limaye, A. S., Korme, T., and Okello, L.: The coupled routing and
1274 excess storage (CREST) distributed hydrological model, *Hydrol. Sci. J.*, 56, 84–98,
1275 <https://doi.org/10.1080/02626667.2010.543087>, 2011.
1276
1277 Wasko, C. and Guo, D.: Understanding event runoff coefficient variability across Australia
1278 using the hydroEvents R package, *Hydrol. Process.*, 36, e14563,
1279 <https://doi.org/10.1002/hyp.14563>, 2022.
1280
1281 Wasko, C., Guo, D., Ho, M., Nathan, R., and Vogel, E.: Diverging projections for flood and
1282 rainfall frequency curves, *J. Hydrol.*, 620, 129403,
1283 <https://doi.org/10.1016/j.jhydrol.2023.129403>, 2023.
1284
1285 Zittis, G., Bruggeman, A., and Lelieveld, J.: Revisiting future extreme precipitation trends in
1286 the Mediterranean, *Weather Clim. Extrem.*, 34, 100380,
1287 <https://doi.org/10.1016/j.wace.2021.100380>, 2021.
1288
1289